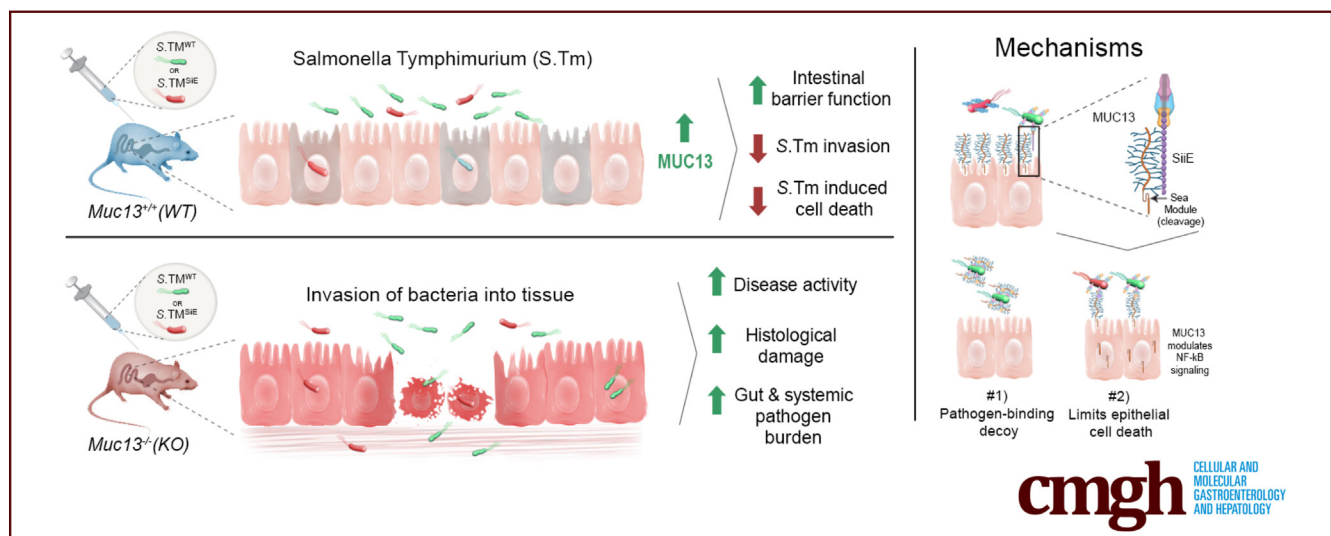


ORIGINAL RESEARCH

MUC13 Cell Surface Mucin Limits *Salmonella Typhimurium* Infection by Protecting the Mucosal Epithelial Barrier

Michael A. McGuckin,^{1,2} Julie M. Davies,³ Pascal Felgner,^{4,5} Kuan Yau Wong,¹ Rabina Giri,³ Yaowu He,⁶ Md Moniruzzaman,^{3,7} Thomas Kryza,⁶ Hareshh Sajiir,¹ John D. Hooper,⁶ Timothy H. Florin,³ Jakob Begun,³ Abderrahim Oussalah,^{8,9,10} Sumaira Z. Hasnain,¹ Michael Hensel,^{4,5} and Yong H. Sheng^{1,11}

¹Inflammatory Disease Biology and Therapeutics Group, Mater Research Institute – The University of Queensland, Translational Research Institute, Woolloongabba, Queensland, Australia; ²Faculty of Medicine Dentistry and Health Sciences, University of Melbourne, Parkville, Victoria, Australia; ³Inflammatory Bowel Diseases Group, Mater Research Institute – The University of Queensland, Translational Research Institute, Woolloongabba, Queensland, Australia; ⁴CellNanOs, Center for Cellular Nanoanalytics, Osnabrueck, Germany; ⁵Division Microbiology, Universitaet Osnabrueck, Osnabrueck, Germany; ⁶Cancer Biology Group, Mater Research Institute-University of Queensland, Woolloongabba, Queensland, Australia; ⁷School of Pharmacy, The University of Queensland, Woolloongabba, Queensland, Australia; ⁸Department of Molecular Medicine, Division of Biochemistry, Molecular Biology, Nutrition, and Metabolism, University Hospital of Nancy, Nancy, France; ⁹University of Lorraine, INSERM UMR_S 1256, Nutrition, Genetics, and Environmental Risk Exposure (NGERE), Faculty of Medicine of Nancy, Nancy, France; ¹⁰Reference Center for Inborn Errors of Metabolism (ORPHA67872), University Hospital of Nancy, Nancy, France; and ¹¹Laboratory of B-Lymphocytes in Autoimmunity and Malignancies, QIMR Berghofer Medical Research Institute, Herston, Queensland, Australia



SUMMARY

We show that MUC13 limits *Salmonella typhimurium* infection. MUC13 maintains barrier integrity by acting as a releasable decoy to limit bacterial invasion and by reducing pathogen-induced cell death. This finding may lead to a novel therapy to treat *S Tm* infection.

BACKGROUND & AIMS: MUC13 cell surface mucin is highly expressed on the mucosal surface throughout the intestine, yet its role against bacterial infection is unknown. We investigated how MUC13 impacts *Salmonella typhimurium* (*S Tm*) infection and elucidated its mechanisms of action.

METHODS: *Muc13*^{-/-} and wild-type littermate mice were gavage with 2 isogenic strains of *S Tm* after pre-conditioning with streptomycin. We assessed clinical parameters, cecal histology, local and systemic bacterial load, and proinflammatory cytokines after infection. Cecal enteroids and epithelial cell lines were used to evaluate the mechanism of MUC13 activity after infection. The interaction between bacterial SiiE and MUC13 was assessed by using siiE-deficient *Salmonella*.

RESULTS: *S Tm*-infected *Muc13*^{-/-} mice had increased disease activity, histologic damage, and higher local and systemic bacterial loads. Mechanistically, we found that *S Tm* binds to MUC13 through its giant SiiE adhesin and that MUC13 acts as a pathogen-binding decoy shed from the epithelial cell surface after pathogen engagement, limiting bacterial invasion. In addition, MUC13 reduces epithelial cell death and intestinal

barrier breakdown by enhancing nuclear factor kappa B signaling during infection, independent of its decoy function.

CONCLUSIONS: We show for the first time that MUC13 plays a critical role in antimicrobial defense against pathogenic *S Tm* at the intestinal mucosal surface by both acting as a releasable decoy limiting bacterial invasion and reducing pathogen-induced cell death. This further implicates the cell surface mucin family in mucosal defense from bacterial infection. (*Cell Mol Gastroenterol Hepatol* 2023;16:985–1009; <https://doi.org/10.1016/j.jcmgh.2023.08.011>)

Keywords: Salmonella; Bacterial Invasion; Intestinal Barrier; Epithelial Cell; Mucin; MUC13; Adhesion; Cell Death.

Salmonella enterica subspecies I serovar typhimurium (*S Tm*) is a leading cause of foodborne illness. Estimated cases exceed 93 million, with 155,000 deaths reported worldwide annually.¹ At the early infection stage, the intestinal barrier is breached primarily through direct infection of barrier-forming epithelial cells. Understanding how the cellular and molecular interaction between the pathogen and epithelial cells influences disease outcomes may lead to the design of new therapies to prevent or treat *Salmonella* infection.

S Tm is a facultative intracellular Gram-negative pathogen that has developed powerful strategies to infect the gastrointestinal tract. A key feature of this bacterium is the ability to invade non-phagocytic cells. Entry of *S Tm* into the brush border of intestinal epithelial cells (IECs) is an important virulence trait that precipitates intestinal inflammation and systemic dissemination. *S Tm* invasiveness is mediated by its type 3 secretion system (T3SS) including T3SS-1 and T3SS-2, encoded by pathogenicity island 1 (SPI1) and SPI2, respectively.^{2–5} T3SS is a molecular syringe that injects virulence effector proteins directly into the cytosol of host cells. These effectors (such as SipA, SipC, SopE/SopE2, and SopB) cooperatively manipulate multiple host signaling pathways to induce rapid actin polymerization and membrane ruffling, further facilitating bacterial internalization.^{6–9}

S Tm not only relies on these injected effectors but also uses several other T3SS-independent mechanisms to enter host cells.^{10,11} They are equipped with many adhesion proteins that can be subdivided into fimbrial adhesins (eg, Fim fimbriae, Curli), autotransporter adhesins (eg, MisL, SadA), and type 1 secretion system (T1SS) substrates (eg, BapA, SiiE).¹² The *Salmonella* giant adhesin SiiE is a key factor in the apical invasion of polarized epithelial cells.^{13,14} SiiE is encoded by pathogenicity island 4 (SPI4) and mediates *Salmonella* binding to the apical surface of polarized epithelial cells.¹⁵ *S Tm* uses the cooperative activity of T3SS and T1SS substrate adhesin SiiE to invade polarized epithelial cells.^{16,17}


S Tm infection causes substantial epithelial cell death during early infection.^{18–20} Whether cell death is a host-driven defensive strategy to limit bacterial replication or a bacterial strategy driving its systemic dissemination remains to be elucidated.²¹

Intestinal mucosal epithelial cells form a contiguous physical barrier reinforced by a surface layer of glycocalyx and a secreted layer of mucus to physically exclude most bacteria from cell surface contact.^{22,23} Secreted and cell-surface mucins are large glycoproteins covered with a dense array of complex O-linked oligosaccharides and are the major constituent of the mucus barrier and the glycocalyx, respectively.²² In addition to protection, membrane-anchored cell-surface mucins participate in intracellular signal transduction and play an important role in the survival and regeneration of mucosal epithelial cells.^{24,25} Although the MUC1 cell surface mucin can play a protective role against some gastrointestinal pathogens, such as *Campylobacter jejuni*²⁶ and *H. pylori*,^{27,28} it can facilitate *Salmonella* invasion by acting as a receptor for the *Salmonella* SiiE adhesin,²⁹ which is in contrast to its protective role. However, the role of other cell surface mucins in infection has not been empirically studied.

The MUC13 cell surface mucin is highly induced by bacterial and malaria parasite infections.^{30,31} Normally, the MUC13 protein is found on the apical surface of intestinal enterocytes and goblet cells, but it can also be shed from the surface.³² During infection and inflammation, MUC13 cytoplasmic expression is increased, likely reflecting immune-driven enhanced biosynthesis to compensate for shedding from the cell surface.^{25,33,34} We have previously shown that MUC13 plays a critical role in protecting intestinal epithelial cells from death in response to a range of triggers, rendering *Muc13*-deficient mice more susceptible to chemically induced colitis.²⁵ The increased susceptibility to DSS-induced colitis in *Muc13*-deficient mice could suggest that MUC13 has a role in intestinal barrier function during attack by pathogens.

MUC13 contains a mucin extracellular domain consisting of a tandem repeat region rich in proline, threonine, and serine that is O-glycosylated. Although MUC13 lacks the canonical sea urchin sperm protein enterokinase and agrin (SEA) domain cleavage site GSVV motif,³⁵ it does have other essential structural features of the SEA domain.³² Biochemical analysis from 2 independent laboratories supports the notion that MUC13 undergoes cleavage within the SEA domain.^{32,36} Furthermore, multiple proteomic analyses have confirmed that MUC13 is a significant component of secreted mucus,^{37,38} indicating that MUC13 is likely

Abbreviations used in this paper: BME, Basement Membrane Matrix; CFU, colony-forming unit; DAI, disease activity index scores; d.p.i, day post-infection; FITC, fluorescein isothiocyanate; h.p.i, hours post-infection; IEC, intestinal epithelial cell; MLN, mesenteric lymph node; NF- κ B, nuclear factor kappa B; PBS, phosphate-buffered saline; SEA, sea urchin sperm protein enterokinase and agrin; SEM, standard error of the mean; T3SS, type 3 secretion system; TUNEL, terminal deoxynucleotidyl transferase-mediated dUTP nick-end labeling; WT, wild-type.

 Most current article

© 2023 The Authors. Published by Elsevier Inc. on behalf of the AGA Institute. This is an open access article under the CC BY-NC-ND license (<http://creativecommons.org/licenses/by-nc-nd/4.0/>).

2352-345X

<https://doi.org/10.1016/j.jcmgh.2023.08.011>

autocatalytically cleaved at an unknown sequence during protein folding in the endoplasmic reticulum.

It also has a 69 amino acid cytoplasmic domain that includes 8 serine and 2 tyrosine residues for potential phosphorylation and a protein kinase C consensus phosphorylation motif likely to be involved in signaling pathways regulating cell death and proliferation.^{25,32,39} The extracellular domain of MUC13 expresses diverse and complex O-linked oligosaccharides including terminal sialylated and sulfated glycans.^{32,40} This is a common feature of mucins; they often present diverse oligosaccharide structures in the glycocalyx that pathogens have evolved to bind. Because MUC13 is highly expressed on the apical surface of intestine epithelial cells in both humans and mice, it may mediate direct contact between the host and invading pathogens attempting to bind to the glycocalyx. *MUC13* polymorphisms are also significantly associated with susceptibility to enterotoxigenic *Escherichia coli* infection in pigs.⁴¹ However, there is some uncertainty, and it has been suggested that rather than *MUC13*, it is a neighboring gene that is involved in the reported *E coli* susceptibility.⁴² Further analysis also suggests that piglet susceptibility to enterotoxigenic *E coli* is not related to the expression level of MUC13, with polymorphisms affecting the function rather than the level of expression.^{43,44} Thus, the role of MUC13 during gastrointestinal bacterial infection remains unclear.

Here we report that MUC13 inhibits *S Tm* infection by acting as a pathogen-binding releasable decoy molecule and prevents tissue damage by inhibiting excessive cell death and barrier breakdown. Thus, MUC13 plays a crucial role in host defense against *S Tm* infection.

Results

Intestinal Expression of MUC13 Is Rapidly Up-regulated in Response to *Salmonella* Infection

MUC2 is a secreted mucin and the major constituent of the intestinal mucus layer that functions as a physical barrier to pathogens like *S Tm*,^{45,46} and its expression is increased after infection.⁴⁶ In comparison, little is known of the function and regulation of cell surface mucins in response to *S Tm*. Therefore, we determined the expression of MUC13 in response to *S Tm* infection in vivo by using the streptomycin pretreated mouse model.⁴⁷ The streptomycin-pretreatment mouse model of *Salmonella* infection provides a robust means to study pathogen-host interplay during enteric disease in genetically tractable animals.⁴⁷ In the uninfected cecum and colon, strong MUC13 staining was identified on the apical surface of epithelium with weak cytoplasmic staining (Figure 1A and B). Within 24 hours of infection, there was a strong induction of MUC13 expression in the cecum, with an intense expression on the cell surface and in the cytoplasm that was maintained for 3 days (Figure 1A). A similar expression pattern to the cecum was observed in the colon (Figure 1B). The follicle-associated epithelium cells in cecal patches were also strongly positive for Muc13 staining (Figure 1C). Strong MUC13 expression was also present in the cecal patch epithelium (Figure 1C). This site has a role in antigen sampling from the

luminal content, similar to Peyer's patches, and is a major site of *S Tm* infection.⁴⁸ Strongly positive MUC13 cells shed into the cecal lumen were observed in infected mice (Figure 1C). We confirmed that the staining of the anti-MUC13 antibody is specific because we did not detect staining with *Muc13*^{-/-} mice or with the secondary antibody (Figure 1D). There was a significant and progressive increase in the level of *Muc13* gene expression over the course of infection in both the cecum and colon (Figure 1E), although the larger increase in protein relative to mRNA at day 1 is suggestive of a rapid post-transcriptional regulation.

Muc13^{-/-} Mice Are More Susceptible to *Salmonella* Infection

The increased expression level of MUC13 in response to *S Tm* suggests that MUC13 is a part of the early epithelial response to infection. To investigate the significance of MUC13 for host defense in vivo, we infected wild-type (WT) and *Muc13*^{-/-} littermate mice as in Figure 1. *Muc13*-deficient mice exhibited more severe clinical signs of infection than WT littermates at 1 day post-infection (d.p.i.) as reflected by a greater loss of body weight and higher disease activity index scores (DAI) (combined scores for loss of body weight, diarrhea, and behavior/activity) (Figure 2A and B). Ex vivo assessment of the infected colons demonstrated a significantly reduced colon length in *Muc13*^{-/-} compared with WT littermate mice at both day 1 and day 3 of the infection (Figure 2C). Infected *Muc13*^{-/-} mice also had significantly greater (2.1-fold at day 1 and 3.8-fold at day 3) intestinal permeability as determined by fluorescein isothiocyanate (FITC)-dextran uptake (Figure 2D). Similar results were obtained with the *S Tm* NCTC strain (Figure 2E-H).

In agreement with the clinical observations, *Muc13*^{-/-} mice showed more severe histologic damage and inflammation in the cecum in response to *S Tm* than WT littermates (Figure 3). By 1 d.p.i., *Muc13*^{-/-} mice exhibited significantly increased epithelial damage and a trend of a higher level of inflammation compared with WT mice (Figure 3A). By 3 d.p.i., these mice demonstrated a significant increase in epithelial damage and a significant elevation in inflammation when compared with WT mice (Figure 3B). These data indicate that MUC13 protects against epithelial damage and the associated inflammatory response during *Salmonella* infection.

MUC13 Limits *S Tm* Expansion and Penetration of the Intestinal Barrier

Next, we examined the *S Tm* distribution within the intestinal tract and counted live bacteria within gastrointestinal and systemic tissues. We observed that stool *S Tm* burden was significantly higher in *Muc13*^{-/-} mice throughout the infection period (Figure 4A). Detection of bioluminescent bacteria showed the highest density in the cecum in both WT and *Muc13*^{-/-} mice at 1 d.p.i. (Figure 4B and C), consistent with previous findings that the cecum is the major site of *S Tm* infection.⁴⁷ Limiting dilution culture

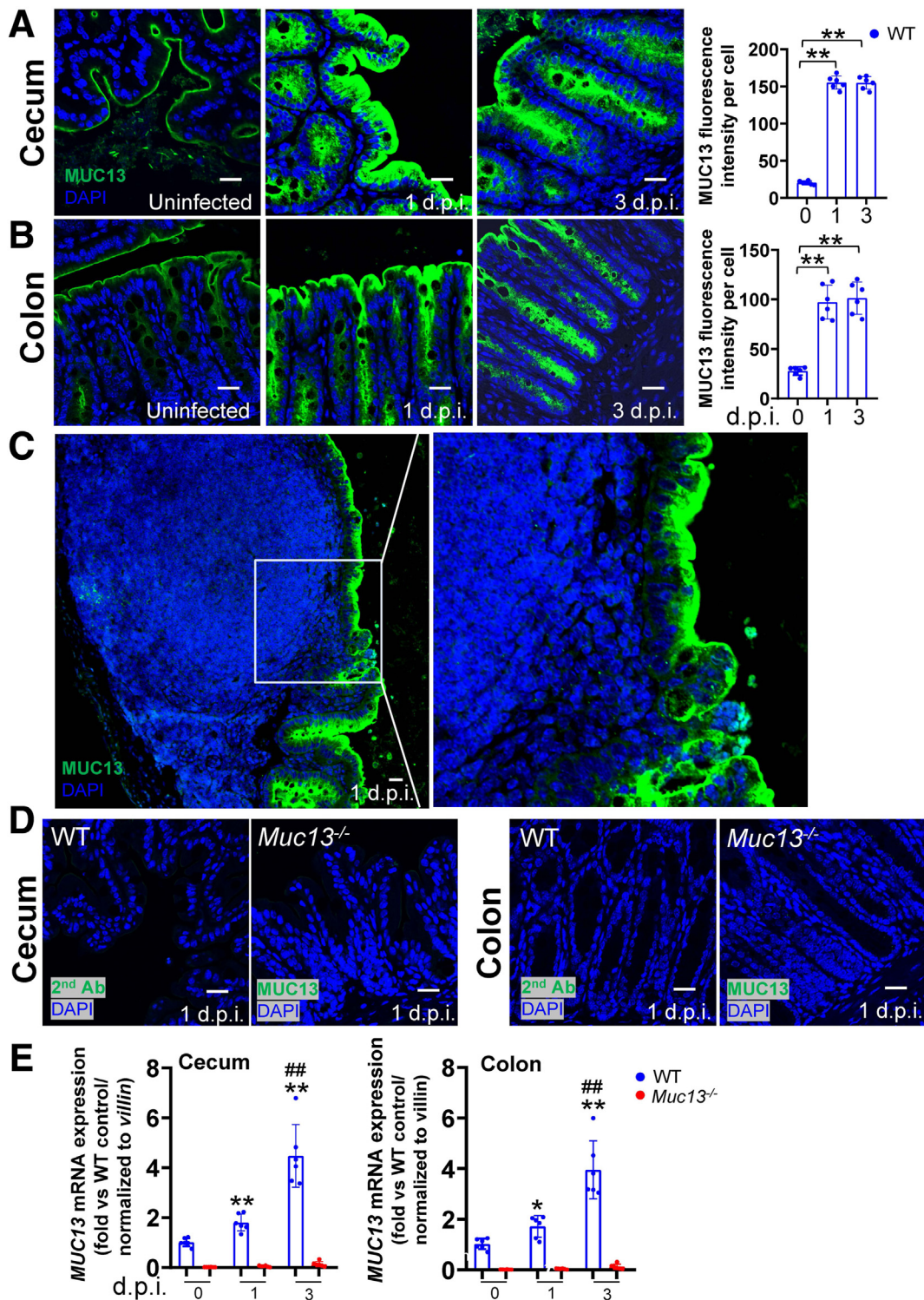


Figure 1. Intestinal MUC13 expression is rapidly induced by *S Tm* infection. *Muc13*^{+/+} (WT) C57BL/6 littermate mice were administered streptomycin (20 mg/mouse, orally gavaged [o.g.]) 24 hours before being uninfected (PBS) or infected by o.g. with 4×10^7 CFU of *S Tm* SL1344. The mice were killed and sampled at 1 d.p.i. (n = 6) or 3 d.p.i. (n = 6). (A–C) Immunofluorescence staining for MUC13 (green) and nuclei (DAPI, blue) in the cecum (A) or colon (B) of WT mice. Left panel: representative immunofluorescence images; 20 μ m scale bars shown. Right panel: fluorescence intensity of MUC13 was determined by ImageJ software in at least 25 individual epithelial cells per mouse. The average intensity was plotted. (C) Immunofluorescence staining for MUC13 (green) and nuclei (DAPI, blue) in the cecal patches. 20 μ m scale bars are shown. (D) Immunofluorescence staining for second Ab (green) and nuclei (DAPI, blue) in the cecum or colon of WT mice, or MUC13 (green) and nuclei (DAPI, blue) in *Muc13*^{-/-} mice. 20 μ m scale bars are shown. (E) *Muc13*^{-/-} or WT littermates were treated as in A and B. *Muc13* mRNA expression in the cecum (left) or colon (right) was determined by quantitative real-time polymerase chain reaction (n = 6). Statistics: (A, B, and E) individual data points, mean \pm standard error of the mean (SEM), Mann Whitney U test, WT mice, *1 or 3 d.p.i. vs uninfected, #3 d.p.i. vs 1 d.p.i., **P* < .05, ***P* < .01, ###*P* < .01. Data are representative of 2 independent experiments.

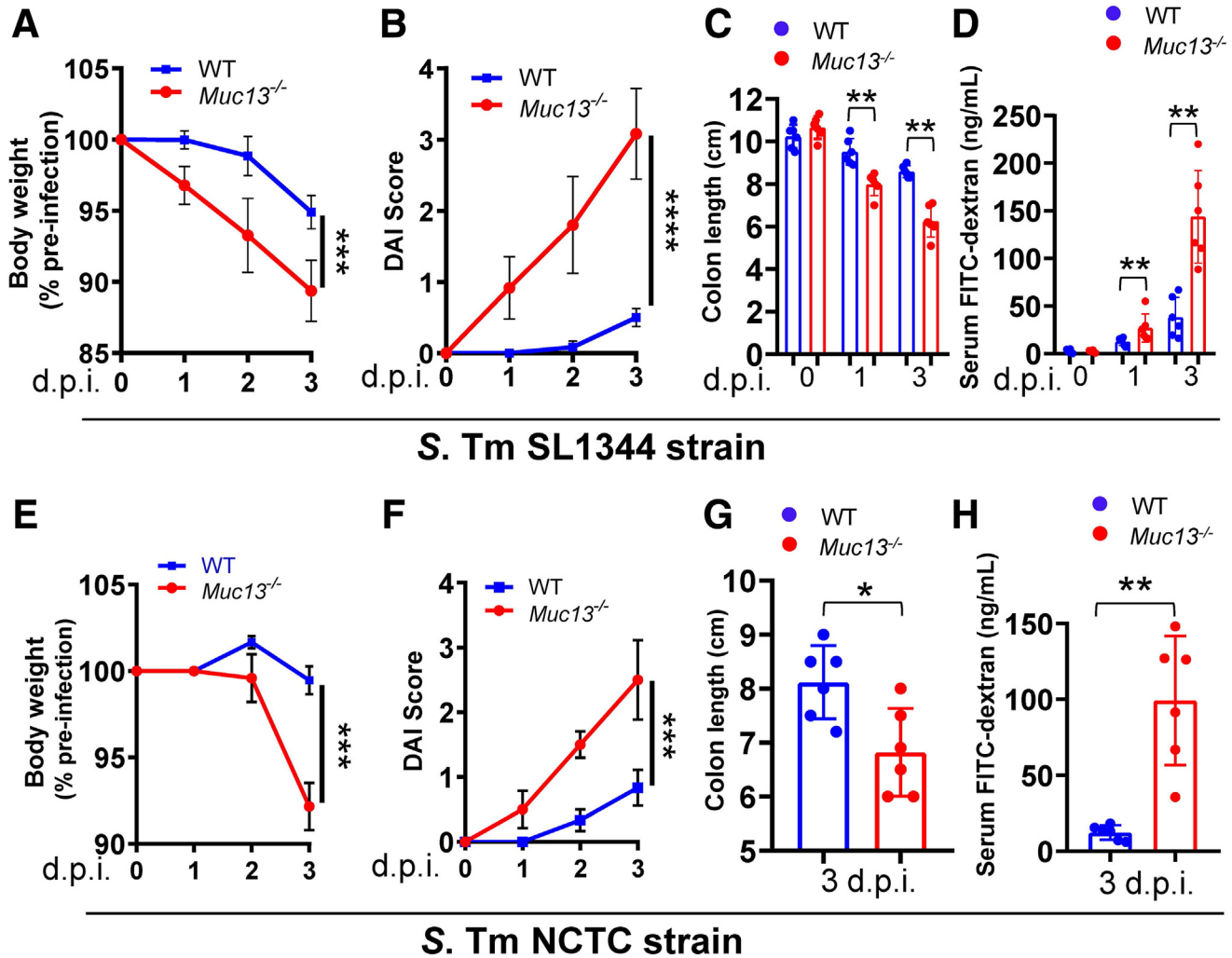


Figure 2. *Muc13*^{-/-} mice are more susceptible to *S Tm* infection. *Muc13*^{-/-} and *Muc13*^{+/+} (WT) C57BL/6 littermate mice were infected as described in Figure 1 with *S Tm* SL1344 strain (A–D, n = 6) or *S Tm* NCTC strain (E–H, n = 6). (A and E) Body weight from 0 to 3 d.p.i. expressed as percentage of pre-infected body weight. (B and F) Clinical DAI scores (aggregate scores for loss of body weight, diarrhea, inactivity, shivering, and hunched posture) were assessed daily for 3 days. (C and G) Colon length at indicated d.p.i. (D and H) FITC-dextran intestinal permeability assay at indicated d.p.i. Statistics: (A, B, E, and F) Two-way analysis of variance with Geisser Greenhouse correction; (C, D, G, and H) individual data points, mean ± SEM, Mann-Whitney *U* test, *Muc13*^{-/-} vs WT mice; **P* < .05, ***P* < .01. Data are representative of 3 independent experiments.

confirmed the cecum had the highest density of bacteria at 1 d.p.i. and revealed ~10-fold higher *S Tm* burden in the ceca, small intestine, and colon of *Muc13*^{-/-} mice compared with WT mice (Figure 4D). Rapid translocation of *S Tm* through the intestine was also observed at 1 d.p.i., with bacteria reaching the mesenteric lymph nodes (MLNs), spleen, and liver in all *Muc13*^{-/-} mice, compared with only 2 of 6 WT mice (Figure 4D). As infection progressed to 3 d.p.i., *Muc13*^{-/-} mice maintained ~10-fold greater levels of *S Tm* burden in the ceca, small intestine, and colon (Figure 4E). Similarly, we observed ~10-fold higher *S Tm* burden in the MLNs, spleen, and liver of *Muc13*^{-/-} mice (Figure 4E). Similar results were obtained with the *S Tm* NCTC strain (Figure 4F). These data suggest that there is an increase in bacteria in both the lumen and mucosal tissue of *Muc13*-deficient mice. In the cecum of *Muc13*^{-/-}

mice, *S Tm* proliferates more rapidly and penetrates the intestinal barrier, which is consistent with the histologic findings of greater epithelial damage and widespread inflammation.

MUC13 Acts as a Physical Barrier to Protect Intestinal Epithelium During S Tm Infection

On the basis of both the strong induction of MUC13 in the cecum in response to *S Tm* infection and the enhanced epithelial damage and bacterial penetration in *Muc13*-deficient mice, we hypothesized that MUC13 acts as a protective physical barrier limiting *S Tm* interaction with and penetration of the epithelium. Cell surface epithelial barrier function would be particularly important in the cecum, which lacks a continuous thick mucus layer, leaving the

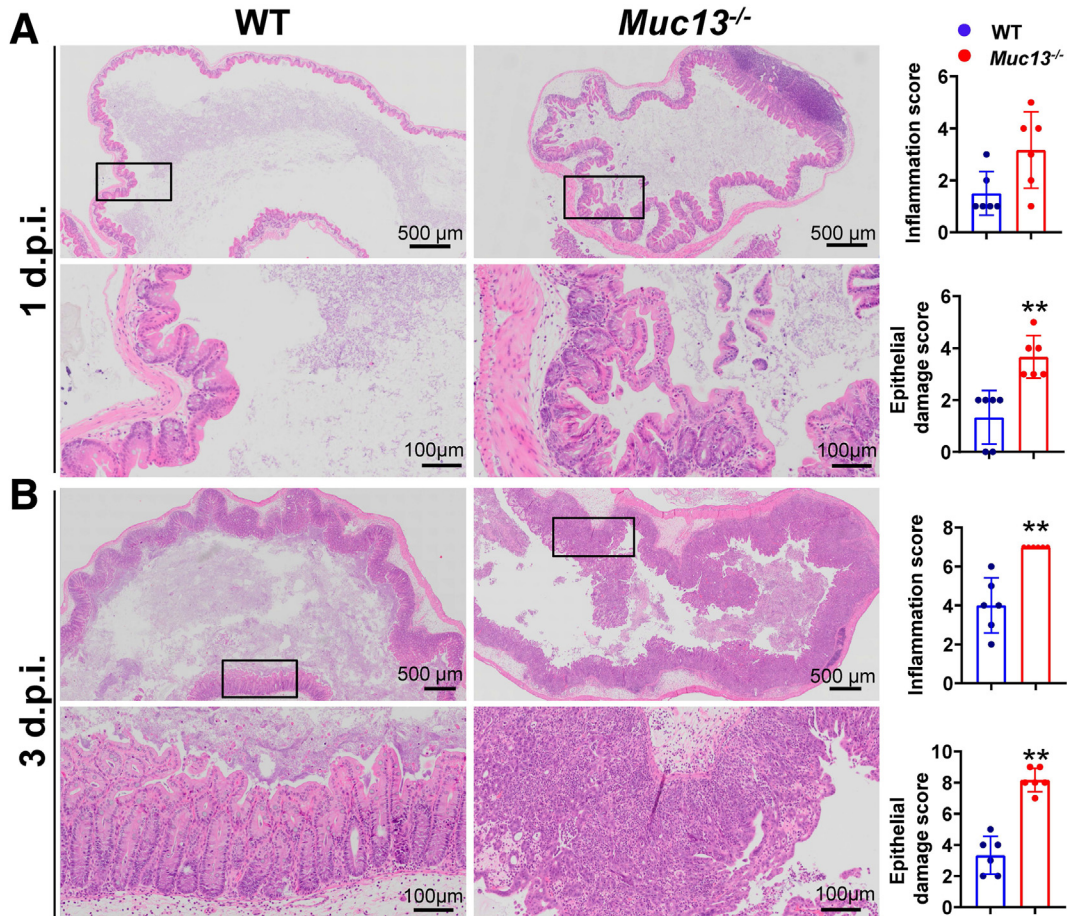


Figure 3. *Muc13*^{-/-} mice showed more severe histologic damage and inflammation. *Muc13*^{-/-} (n = 6) or WT littermate (n = 6) mice were infected with *S Tm* SL1344 as described in Figure 1. H&E-stained cecal sections from representative mice, scale bars as indicated (left). Histologic scores grading severity of inflammation and tissue damage at 1 (A) and 3 (B) d.p.i. (right). Statistics: individual data points, mean ± SEM, Mann-Whitney *U* test, *Muc13*^{-/-} vs WT mice; **P* < .05, ***P* < .01. Data are representative of 3 independent experiments.

epithelial surface of crypts more exposed than in the colon.⁴⁹ Therefore, we investigated whether the increased sensitivity of *Muc13*^{-/-} mice to *S Tm* challenge was associated with increased attachment of bacteria to the epithelium. We examined intestinal tissue fixed in Carnoy's fixative (which preserves the extracellular mucus layer) for the localization of *S Tm* relative to the mucus layer and epithelium by staining for *S Tm* in combination with MUC2 or MUC13. In line with previous findings,⁴⁹ the cecum of WT mice lacked a continuous, MUC2-positive mucus layer (Figure 5A i). MUC13 was highly expressed in the glycocalyx surface of the cecal epithelial tips, and luminal *S Tm* was frequently coated with shed MUC13 (Figure 5A ii). Because the immunofluorescence staining was conducted by using the available antibody that targets the cytoplasmic domain of MUC13, the luminal MUC13 we identified is likely restricted to membranous fragments and exosomes.

Immunostaining further revealed the luminal and mucosal distribution of *S Tm* was dramatically different between WT and *Muc13*^{-/-} mice (Figures 5B and 6A). At 1 d.p.i. in WT mice the epithelial cell surface was covered with MUC13 and provided a distinct barrier that kept the vast

majority of the *S Tm* within the cecal lumen and effectively distanced from the epithelial surface, with only isolated examples of apparent attachment or invasion (Figures 5B and 6A). In contrast, *S Tm* was found in contiguous clusters along the luminal cell surface in *Muc13*^{-/-} mice, where it had penetrated deeper into the crypts and was found in contact with and in the basal region of numerous epithelial cells and in the submucosa (Figures 5B and 6A). By 3 d.p.i., the cecal epithelium of WT mice remained relatively free of invading *S Tm*, although occasional clusters of bacteria were seen within cells underlying the mucosal epithelium, likely to be macrophages or granulocytes (arrow in Figure 6A). In contrast, *Muc13*^{-/-} mice had a significantly higher number of *S Tm* contacting epithelial cells in the mucosa (Figure 5B). There was also extensive shedding of epithelial cells into the lumen that were heavily laden with *Salmonella* (Figure 5B).

Salmonella infection was accompanied by altered mRNA expression of proinflammatory cytokines and antimicrobial factors, including interleukin 22, Reg3γ, lipocalin-2, and S100 molecules, in the cecum of both WT and *Muc13*^{-/-} mice (Figure 6B). In contrast, B-defensin expression was markedly reduced by infection in the cecum of both WT and

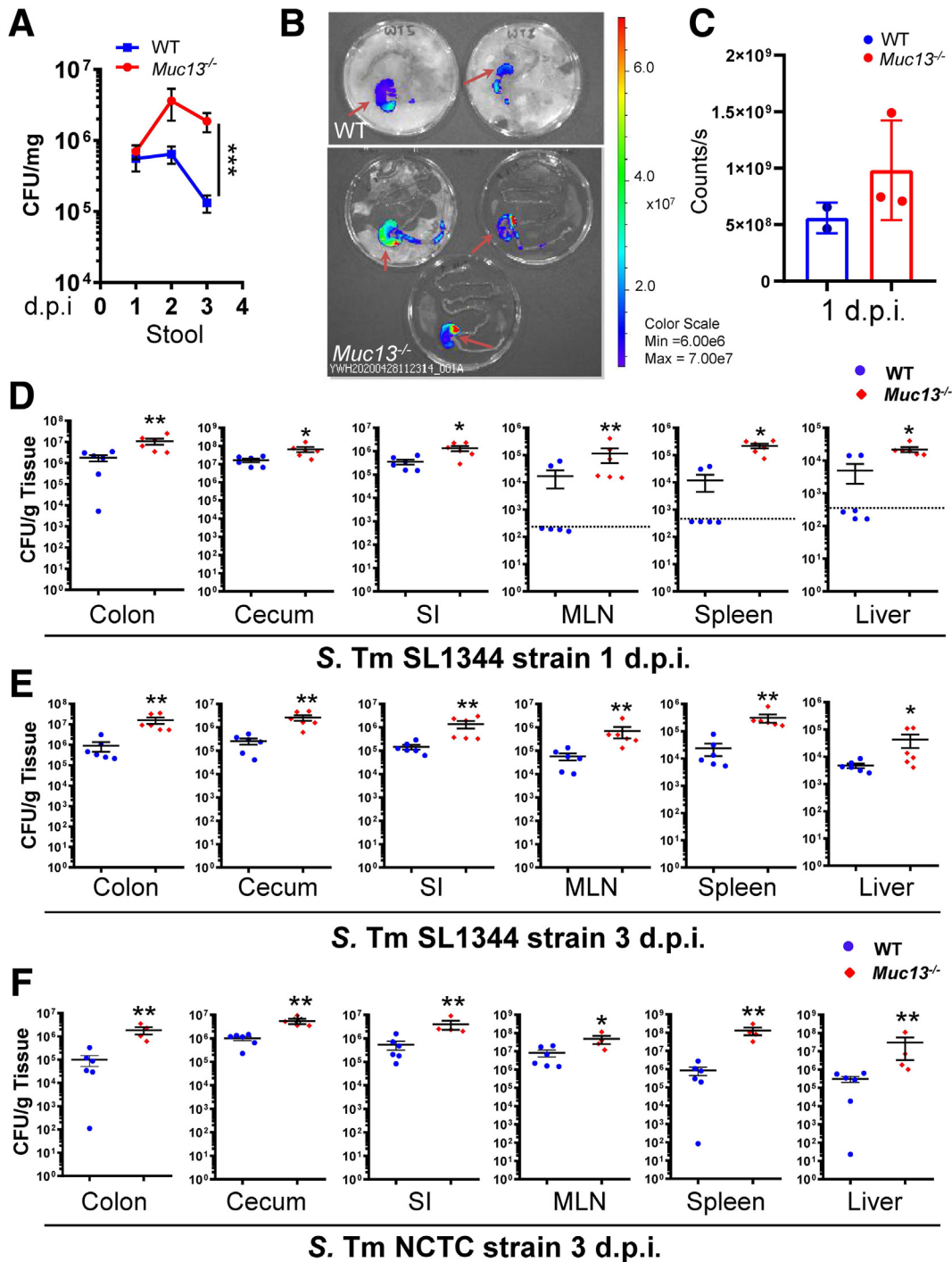


Figure 4. *Muc13*^{-/-} mice carry higher *S. Tm* burdens in intestinal tissues, MLNs, spleen, and liver than WT mice. (A and B) *Muc13*^{-/-} (n = 3) or WT littermate (n = 2) mice were infected for 1 day with bioluminescent strain of *S. Tm* SL1344 as described in Figure 1. (A) Ex vivo imaging and (B) quantification of total bioluminescence (see color scale) in the gut of infected mice. Arrows indicate the cecum. (C–E) *Muc13*^{-/-} (n = 6) or WT littermate (n = 6) mice were infected with *S. Tm* SL1344 as described in Figure 1. (C) CFUs of *S. Tm* SL 1344 in the stool of mice were determined by limiting dilution culture during infection. (D and E) CFUs of *S. Tm* SL 134 in homogenized gastrointestinal and systemic tissues (SI, small intestine) of mice were determined by limiting dilution culture at 1 (D) and 3 (E) d.p.i.; dashed line, limit of detection. (F) *Muc13*^{-/-} (n = 4) or WT littermate (n = 6) mice were infected with *S. Tm* NCTC as described in Figure 1. CFUs of *S. Tm* NCTC in homogenized gastrointestinal and systemic tissues of mice were determined by limiting dilution culture at 3 d.p.i.; dashed line, limit of detection. Statistics: (B, D, E, and F) mean ± SEM, Mann-Whitney U test, *Muc13*^{-/-} vs WT mice. (C) Two-way analysis of variance with Geisser Greenhouse correction. **P* < .05, ***P* < .01, ****P* < .001. Data are representative of 2 independent experiments.

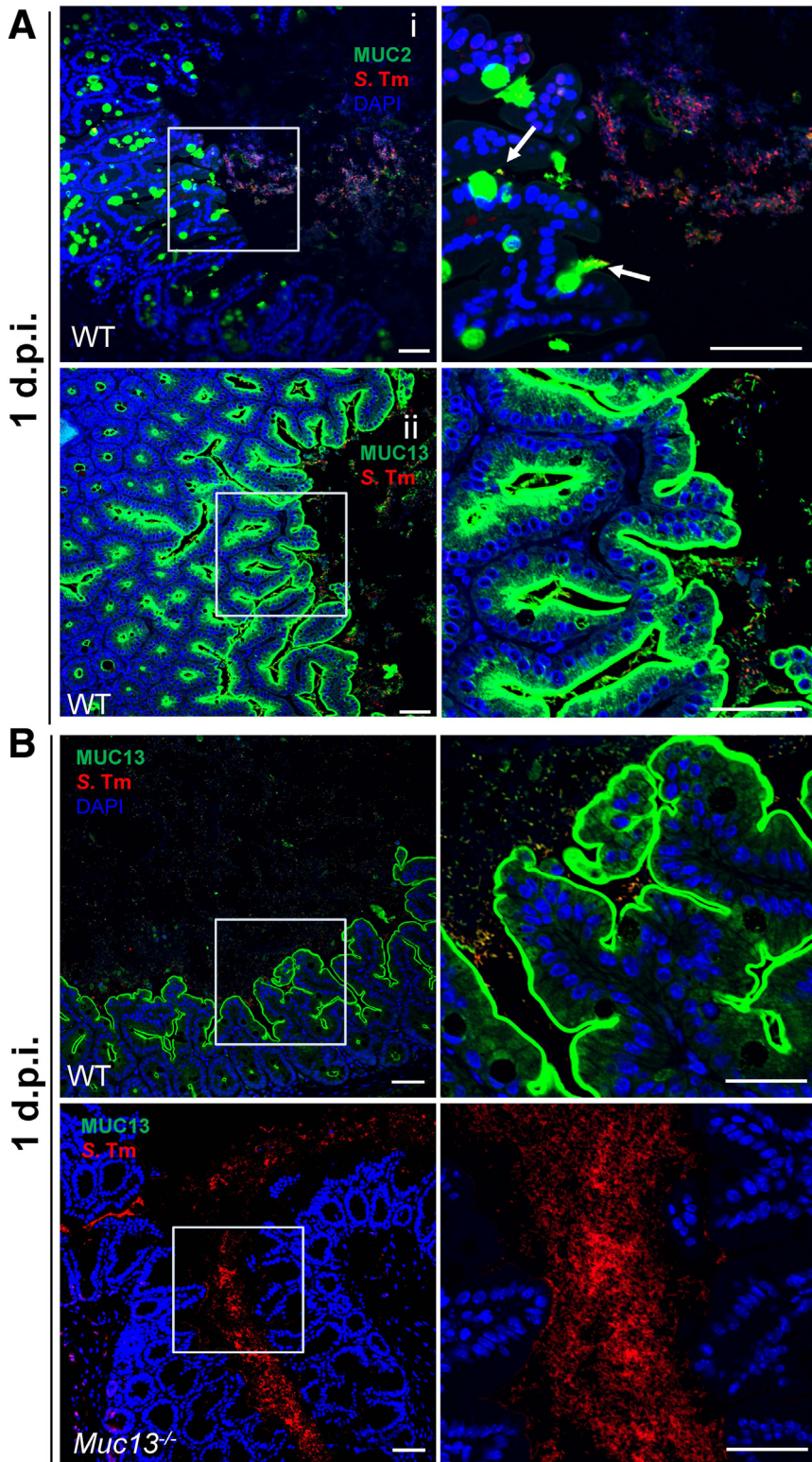


Figure 5. MUC13 acts as a physical barrier to limit *S Tm* contact with cecal surface epithelium. *Muc13*^{-/-} mice (n = 6) or WT littermates (n = 6) were infected with *S Tm* SL1344 as described in Figure 1 and were killed at 1 d.p.i. (A) Representative immunofluorescence image of cecal tissue from WT mice fixed in Carnoy's fixative to preserve mucus and stained for (i) MUC2 (green) and *S Tm* (red); (ii) MUC13 (green) and *S Tm* (red). (Insets show magnification of regions on the right), scale bars = 50 μm. (B) Representative immunofluorescence image of cecal tissue from WT and *Muc13*^{-/-} mice stained for MUC13 (green) and *S Tm* (red) at 1 d.p.i. (Insets show magnified regions on the right), scale bars = 50 μm. Data are representative of 2 independent experiments.

Muc13^{-/-} mice (Figure 6B). Although the magnitude of the expression change of these factors was higher in *Muc13*^{-/-} mice, the temporal pattern was similar to the WT mice, suggesting an alternative type of inflammatory response is

unlikely to underlie the greatly enhanced pathology (Figure 6B). Loss of *Muc13* did not result in compensatory up-regulation of *Muc2* before or after infection and only increased *Muc1* expression by day 3 (Figure 6B),

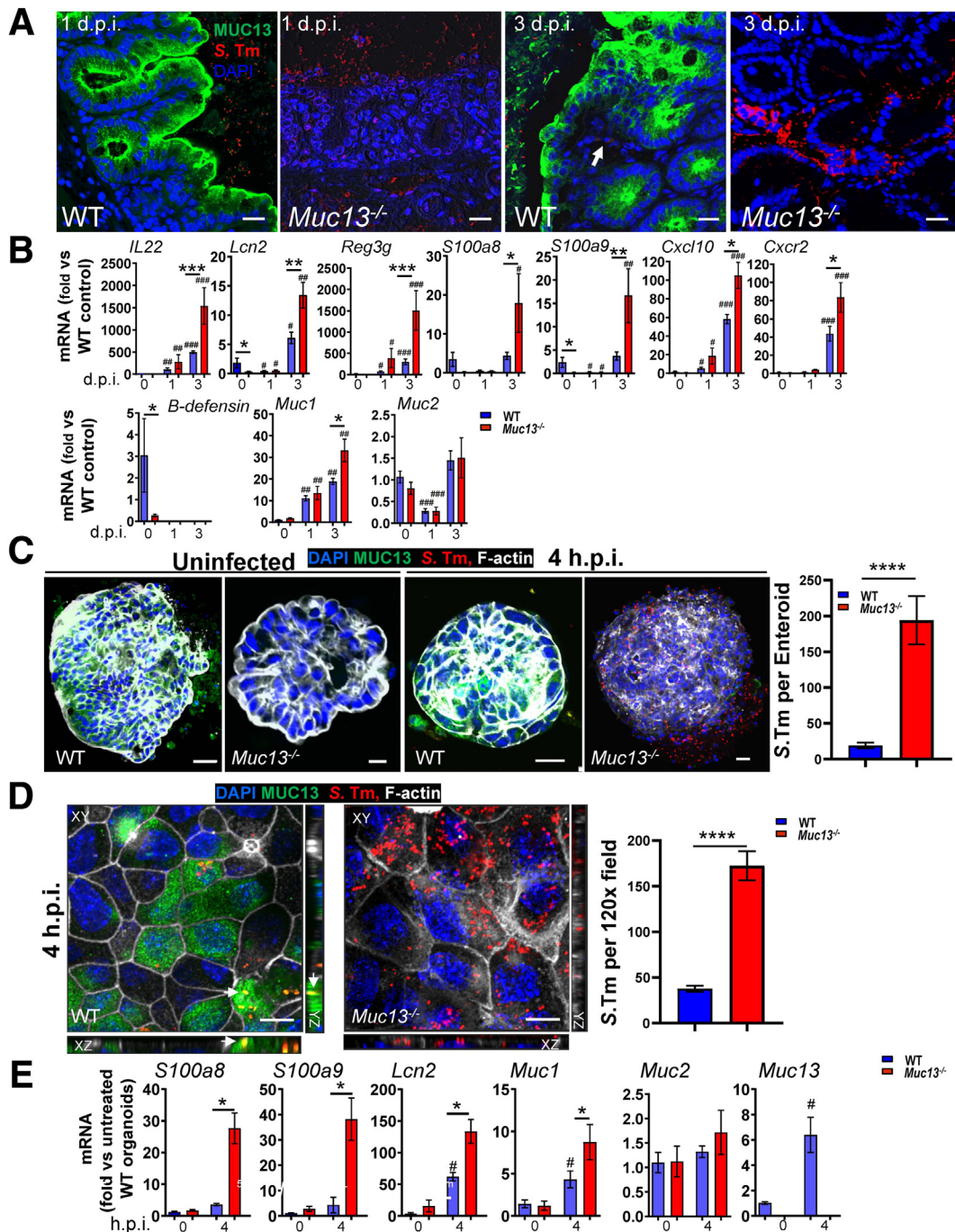


Figure 6. MUC13 acts as a physical barrier to limit *S Tm* contact and reduce inflammation in IEC intrinsic manner.

(A) *Muc13*^{-/-} mice (n = 6) or WT littermates (n = 6) were infected with *S Tm* SL1344 as described in Figure 1 and were killed at 1 or 3 d.p.i. Representative immunofluorescence image of cecal tissue from WT and *Muc13*^{-/-} mice stained for MUC13 (green) and *S Tm* (red) at 1 and 3 d.p.i.; 20 μ m scale bars shown. (B) Quantitative real-time polymerase chain reaction showing cecal expression of indicated proinflammatory and antimicrobial genes, relative to *Hprt*, as well as *Muc1* and *Muc2* genes, relative to villin, at different time points after infection. (C) Cecal enteroids derived from *Muc13*^{-/-} mice (n = 3) or WT littermate mice (n = 3) were maintained in BME for 4 passages. Three days before infection, enteroids were transferred to suspension culture in low-attachment plates and infected with *S Tm* DsRed for 1 hour, followed by gentamicin protection assay. Bacterial colonization was assessed by fluorescence microscopy at 4 h.p.i. Left panel: representative immunofluorescence images; 20 μ m scale bars are shown. Right panel: results are from at least 20 enteroids from each genotype of 3 independent experiments. (D) Cecal enteroid monolayers derived from *Muc13*^{-/-} mice (n = 3) or WT littermate mice (n = 3) were infected with *S Tm* DsRed for 30 minutes, followed by gentamicin protection assay. Bacterial colonization was assessed by fluorescence microscopy at 4 h.p.i. Left panel: representative immunofluorescence images and analysis using IMARIS software; scale bars = 5 μ m. Arrows indicate colocalization of MUC13 with *S Tm*. Right panel: results are from 20 fields of monolayers staining from each genotype of 3 independent experiments. (E) Cecal enteroids were derived as described in C. Quantitative real-time polymerase chain reaction showing cecal organoid expression of indicated antimicrobial genes, relative to *Hprt*, as well as *Muc1*, *Muc2*, and *Muc13* genes, relative to villin, at different time points after infection. Statistics: (B–E) mean \pm SEM, Mann-Whitney U test; **Muc13*^{-/-} vs WT mice or enteroids at same time point, # vs uninfected WT mice or enteroids. * or # $P < .05$; ** or ## $P < .01$, *** or ### $P < .001$, **** $P < .0001$. Data are representative of 3 independent experiments.

demonstrating differential regulation of *Muc1* and *Muc2* during infection. *Muc1* expression was influenced by the absence of *Muc13* expression only at the late stages of infection, likely in response to the greater bacterial burden and inflammatory response.

Taken together, these results demonstrate that *Muc13* deficiency results in enhanced pathogen invasion of the host epithelium, leading to greater penetration into the submucosa and systemic tissues and greater local inflammation.

MUC13 Restrains S Tm Infection in an IEC Intrinsic Manner

To define whether the ability of MUC13 to limit *S Tm* infection in murine ceca reflected an IEC intrinsic role, we infected cecal enteroids. This allowed us to remove confounding factors such as the microbiota or altered immune activity and focus on the function of epithelial cells alone. After establishment, enteroids were induced to reverse polarity to apical side-out by suspension culture⁵⁰; reversal of polarity was consistently observed in these enteroids. Polarized enteroids were then infected with *S Tm* DsRed, and intracellular bacteria were enumerated by using a gentamicin protection assay in combination with fluorescence microscopy. *Muc13*^{-/-} enteroids proved highly susceptible to *S Tm* infection as reflected by higher numbers of *S Tm* infected cells containing microcolonies of intracellular *S Tm* at 4 hours post-infection (h.p.i.) (Figure 6C, Supplementary Figure 1). In contrast, WT enteroids had significantly fewer infected IECs as well as relatively low numbers of intracellular *S Tm* (Figure 6C, Supplementary Figure 1). We also generated two-dimensional monolayer cultures from the murine cecal enteroids and infected them apically with *S Tm* DsRed. Consistent with the observation of polarized enteroids, *Muc13*^{-/-} monolayers proved highly susceptible to *S Tm* infection as evidenced by the high density of attachment and invasion of *S Tm* to the cells and great abundance of colonies compared with WT monolayers at 4 h.p.i. (Figure 6D). The higher intracellular *S Tm* burden in *Muc13*^{-/-} enteroids and two-dimensional monolayers largely mirror the in vivo infection findings that *Muc13*^{-/-} mice show greater invasion of the intestinal epithelium by *S Tm* than WT mice. mRNA expression analysis further demonstrated that there was a significantly greater up-regulation of S100 molecules and lipocalin-2 in the enteroids from *Muc13*^{-/-} than in WT mice, demonstrating greater epithelial-intrinsic responses to the pathogen (Figure 6E). Similar to our in vivo findings, *Muc13* mRNA was significantly increased in response to infection in the WT enteroids. In addition, we found that *Muc1* mRNA expression was significantly up-regulated in *Muc13*^{-/-} enteroids compared with WT enteroids at 4 h.p.i., whereas *Muc2* mRNA expression remained unchanged (Figure 6E). These results support a role for epithelial MUC13 limiting *S Tm* infection.

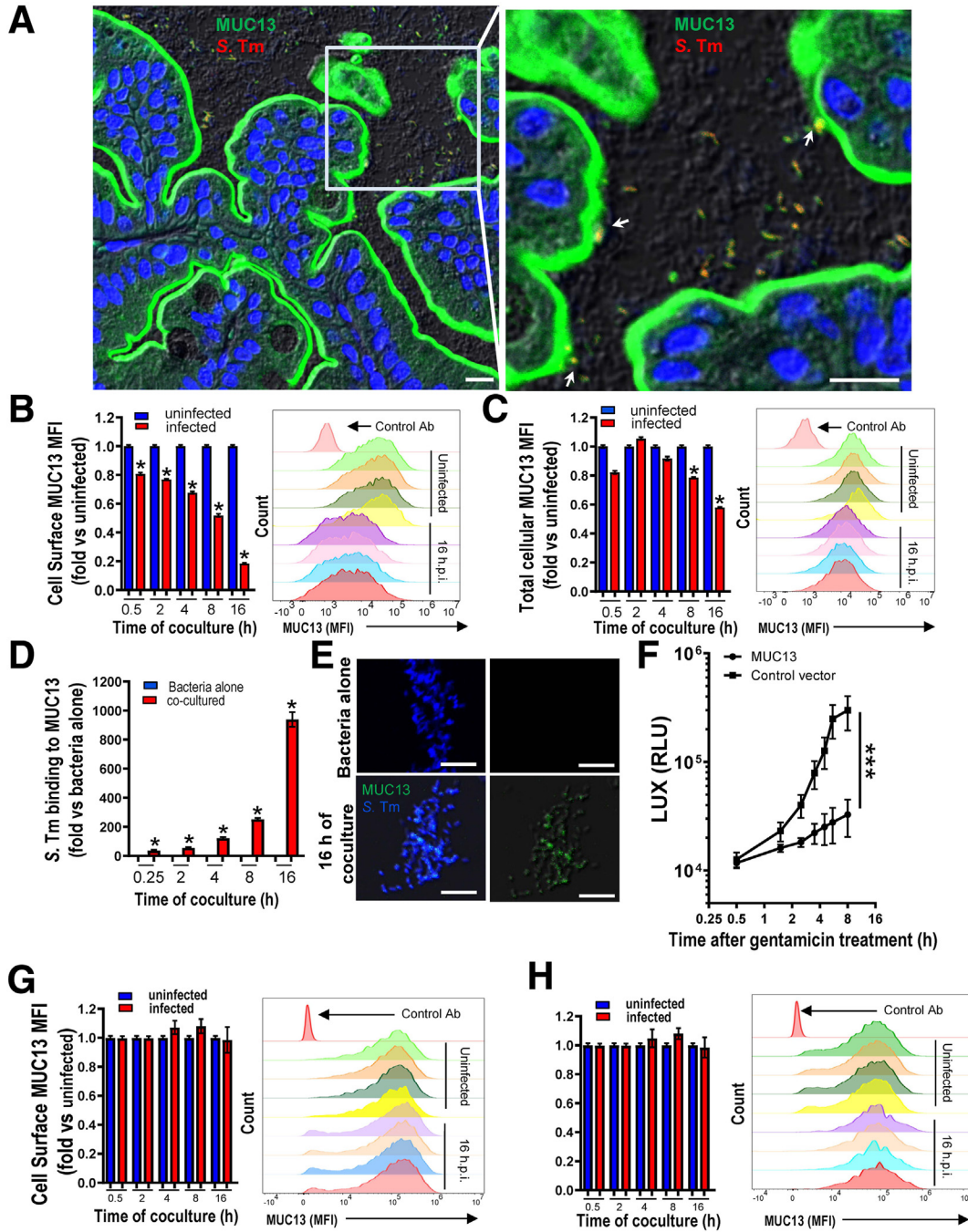
MUC13 Is a Pathogen-Binding Decoy Shed From the Epithelial Cell Surface That Limits Invasion

Because of its abundant expression on the apical surface, we hypothesized that the highly glycosylated extracellular

domain of MUC13 may act as a pathogen-binding decoy like MUC1. MUC1 has previously been shown to act as a releasable decoy and reduce bacterial binding to mucosal epithelial cells.²⁸ Therefore, we investigated whether MUC13 functioned similarly.

We examined cecum tissue for the interaction of *S Tm* with MUC13 by immunostaining. After 1 day of infection, many of the *S Tm* in the lumen were coated with MUC13 in WT mice (Figure 7A). This could have occurred in the lumen by binding secreted MUC13 without epithelial cell engagement, like secretory immunoglobulin A coating of luminal bacteria, or it could have occurred because of the binding to MUC13 on the cell surface, which triggered MUC13 shedding. To assess the effects of MUC13 on attachment of bacteria to the cell surface, we overexpressed MUC13 with a FLAG tag at the N-terminus of the extracellular domain in the human intestinal epithelial cell line SW480, which has low endogenous expression of MUC13³³ under control of the CMV promoter (ie, expressed independently of *MUC13* gene regulation). We then infected confluent monolayers of MUC13-transfected cells with *S Tm* and assessed MUC13 levels over 0.25–16 hours. Cell surface (unfixed cells) and total (fixed and permeabilized) MUC13 were measured by flow cytometry within viable cells with an anti-FLAG antibody. Infection with *S Tm* progressively depleted cell surface MUC13, reaching maximal depletion of ~80% after 16 hours of infection (Figure 7B). At this time, total MUC13 was decreased by ~40% (Figure 7C). Whereas shedding of MUC13 from the infected cell surface exceeded its replacement from the intracellular pool, in these transfected cells it should be noted that MUC13 is regulated by CMV rather than the MUC13 promoter and thus unlikely to be transcriptionally up-regulated in response to infection in the compensatory manner observed with in vivo infection (Figure 1).

To explore whether *S Tm* bound to MUC13 in these co-culture experiments, bacteria recovered from the culture medium were stained for MUC13 using the anti-FLAG antibody reactive with the extracellular domain. MUC13 was detected bound to *S Tm* using both flow cytometry and confocal microscopy (Figure 7D and E). Flow cytometry showed binding of *S Tm* to MUC13 progressively increased from 0.25 hours to 16 hours, reaching ~900-fold increase after 16 hours of infection compared with bacteria alone (Figure 7D). Confocal images showed that MUC13 binding to *S Tm* was often focally intense rather than evenly distributed on the bacterial surface (Figure 7E). We next assessed intracellular replication by using a gentamicin protection assay. *S Tm* was allowed to infect cells for 30 minutes. Gentamicin was then added to the supernatant to kill extracellular bacteria. Gentamicin does not penetrate the cell membrane, so intracellular bacteria are protected and can replicate. MUC13 overexpression reduced intracellular *S Tm* replication (Figure 7F). These results suggest that MUC13 acts as a pathogen-binding decoy shed from the epithelial cell surface after the binding limiting successful adhesion of *S Tm* to the cell surface and subsequent invasion.



S. Tm^{WT} was used for Figure 7A – F, *S. Tm*^{siiE} was used for Figure 7G – H

Figure 7. MUC13 is shed from the luminal epithelial cell surface acting as a pathogen-binding releasable decoy. (A) *Muc13*^{+/+} (WT) mice were infected with *S. Tm* for 1 day as described in Figure 1. Representative immunofluorescence image of cecum tissue stained for Muc13 (green), *S. Tm* (red), and nuclei (blue). Arrows indicate *S. Tm* at the luminal surface staining for MUC13; 10 μm scale bars are shown. (B–H) Vector control and MUC13 overexpressing SW480 human intestinal epithelial cells were co-cultured with WT of *S. Tm* (*S. Tm*^{WT}) (B–F) or with mutant strain of *S. Tm*^{ΔsiiE} (G and H) at multiplicity of infection of 1. Amount of the extracellular domain of MUC13 (α-subunit) per viable cells (B and G) and amount of total cellular α-subunit determined in permeabilized cells (C and H) from uninfected cells or cells co-cultured with *S. Tm*^{WT} or *S. Tm*^{ΔsiiE} for indicated times were measured by flow cytometry using an antibody to detect an N-terminal FLAG tag on the extracellular domain of MUC13. Median fluorescence intensity (MFI) in viable cells was determined after subtraction of the MFI using a negative control antibody and expressed as a fold of the mean MFI of cells from uninfected cultures. Representative flow cytometry histograms are shown. (D and E) In a parallel experiment described in (B and C) the presence of MUC13 on *S. Tm*^{WT} recovered from the conditioned medium of MUC13 expressing SW480 cells was determined by staining with the anti-FLAG antibody or an isotype control, followed by flow cytometry (D) and confocal microscopy. Ten μm scale bars are shown (E). *S. Tm*^{WT} not co-cultured with mammalian cells were used as controls. (F) Vector control and MUC13 overexpressing SW480 cells were co-cultured with bioluminescent strain of *S. Tm*^{WT} at multiplicity of infection of 1. *S. Tm* Lux gentamicin protection assay. Statistics: (B–D and G and H) mean ± SEM, Mann-Whitney *U* test, *n* = 4; (B and C): infected vs uninfected cells; (D): co-cultured vs not co-cultured *S. Tm*. (F) Repeated-measures two-way analysis of variance with Geisser Greenhouse correction, *n* = 4. **P* < .05, ****P* < .001. Data are representative of 2 independent experiments.

Binding of MUC13 to *Salmonella* Is Dependent on the Adhesin SiiE

S Tm binding to receptors on epithelial cells is mediated by multiple adhesin proteins. SiiE is a giant adhesin involved in the binding of *S Tm* to the apical side of epithelial cells. SiiE binds to glycostructures with terminal N-acetylglucosamine and/or α 2,3-linked sialic acid.⁵¹ The tandem repeats of the mucin extracellular domains are highly glycosylated with complex O-linked glycans on which sialic acids are frequently present in the intestine.⁵² To determine whether SiiE is mediating binding to MUC13, we co-cultured confluent monolayers of FLAG-tagged MUC13 overexpressing SW480 cells with *S Tm* ^{Δ siiE} (*S Tm* *siiE* knockout strain) and sampled over 0.25–16 hours. The amount of cell surface and total MUC13 was measured within individual viable cells by flow cytometry as shown in Figure 7B and C. Co-culture with *S Tm* ^{Δ siiE} did not induce surface shedding or alter the total pool of MUC13 up to 16 h.p.i. (Figure 7G and H). Flow cytometry of the bacteria recovered from the culture medium showed that there was no binding of MUC13 to *S Tm* ^{Δ siiE} during the co-culture (Figure 8A). Thus, the bacterial SiiE adhesin is required to induce MUC13 shedding from epithelial cells during infection.

To measure whether MUC13 directly binds to SiiE, we purified shed MUC13 from the supernatants of SW480 MUC13-transfected cells (Figure 8B) and incubated it with *S Tm* in a bacterial aggregation assay. Because MUC13 has many glycostructures and *S Tm* expresses a large amount of SiiE on its surface, we reasoned this would induce agglutination. Indeed, we observed clumping only in the presence of both MUC13 and SiiE (Figure 8C). MUC13-induced clumping was SiiE specific because a strain with deletions of *fim* (type I fimbriae), *flil* (flagella assembly), and SPI4 (*siiE* and cognate T1SS) did not result in clumping, and the clumping was rescued by inducing ectopic expression of *sii* genes in this strain (Figure 8D). Thus, our data indicate that MUC13 can bind directly to SiiE, and the result of this interaction induced aggregation of *S Tm*.

MUC13-SiiE Interaction Only Partly Accounts for MUC13 Protection Against *S Tm* Infection

We next investigated whether MUC13 protects from infection solely through its decoy shedding activity or whether MUC13 provides additional cellular protection. If all the protection provided by MUC13 occurred via shedding, we would expect that WT and *Muc13*^{-/-} mice would have similar disease severity when infected with the SiiE deletion strain of *S Tm*, which does not engage the MUC13 decoy shedding response. To test this, we infected WT and *Muc13*-deficient mice with the *S Tm* ^{Δ siiE}. No difference in body weight loss was observed between the groups (Figure 9A), but *Muc13*-deficient mice exhibited higher disease activity, shorter colons, increased (2.3-fold) intestinal permeability, increased histologic damage, and higher systemic bacteria burden compared with WT littermates (Figures 9B–F and 10A and B). On day 1 of *S Tm* ^{Δ siiE} infection, there was substantial epithelial cell death with sheets of shed epithelial cells in the cecum in *Muc13*^{-/-} mice,

which was not evident in WT mice (Figure 9E). No difference in the *S Tm* ^{Δ siiE} burden was found in the ceca and colons of *Muc13*^{-/-} compared with WT mice (Figure 10A), but there was about 10-fold greater colony-forming units (CFUs) measured in small intestines of *Muc13*^{-/-} vs WT mice. Systemic translocation of *S Tm* ^{Δ siiE} to the MLNs, spleen, and liver was also evident in 6/6 *Muc13*^{-/-} mice, compared with only 2 of 6 WT mice (Figure 10A). By day 3 of *S Tm* ^{Δ siiE} infection, tissue destruction, cell death, submucosa edema, and inflammatory infiltrates were observed in the ceca of *Muc13*^{-/-} mice, which was much less prominent in the WT ceca (Figure 9F). Again, no difference in the burden of *S Tm* ^{Δ siiE} was found in the ceca, small intestine, or colon of *Muc13*^{-/-} and WT mice (Figure 10B). However, systemically we observed ~10-fold higher burden in the MLNs, spleen, and livers of *Muc13*^{-/-} mice compared with WT mice (Figure 10B). Thus, despite not engaging the decoy activity of MUC13, infection with the *S Tm* ^{Δ siiE} was exacerbated in the *Muc13*^{-/-} mice. *S Tm* ^{Δ siiE} mutant can more rapidly and extensively cross the intestinal barrier in *Muc13*^{-/-} mice. This suggests that in mice that are infected with *S Tm* strains that cannot bind to MUC13, MUC13 continues to be protective against infection via a mechanism that is independent of the engagement of the SiiE adhesin and its role as a decoy receptor.

In WT mice we also observed there was a significant up-regulation of MUC13 expression in both the cecum and colon in response to *S Tm* ^{Δ siiE} infection (Figure 10C and D). Increased expression was maintained for 3 days (Figure 10C and D). These results indicate that MUC13 is up-regulated after infection independent of SiiE binding. Taken together, our data indicate that MUC13 affords another layer of protection against *S Tm* infection beyond decoy shedding. The *S Tm* strain that cannot bind to MUC13 still caused more pathology in the *Muc13*^{-/-} mice, demonstrating that MUC13 is a key element of intestinal barrier function for both MUC13-binding and non-MUC13-binding *S Tm*.

MUC13 Protects Intestinal Epithelial Cells From *S Tm*^{WT} and *S Tm* ^{Δ siiE} Induced Cell Death

The increased severity of epithelial damage, including sloughing of sheets of epithelial cells into the lumen, in the absence of MUC13 in response to both *S Tm* and *S Tm* ^{Δ siiE} suggests there is increased death of epithelial cells. Increased cell death could be due to increased bacterial invasion and/or enhanced susceptibility to cell death due to the absence of MUC13 intracellular signalling as we have shown previously.^{25,33} Therefore, we measured the extent of cell death using terminal deoxynucleotidyl transferase-mediated dUTP nick-end labeling (TUNEL) staining on cecal sections. There was no difference in the number of dying cecal epithelial cells between WT and *Muc13*^{-/-} mice before infection (data not shown). Infection with WT of *S Tm* (*S Tm*^{WT}) induced epithelial cell death in both WT and *Muc13*^{-/-} mice; however, the extent of cell death was significantly higher (typically ~4-fold) in the cecum in *Muc13*^{-/-} compared with WT mice after both 1 and 3 d.p.i. (Figure 11A). Because of our previous findings that MUC13

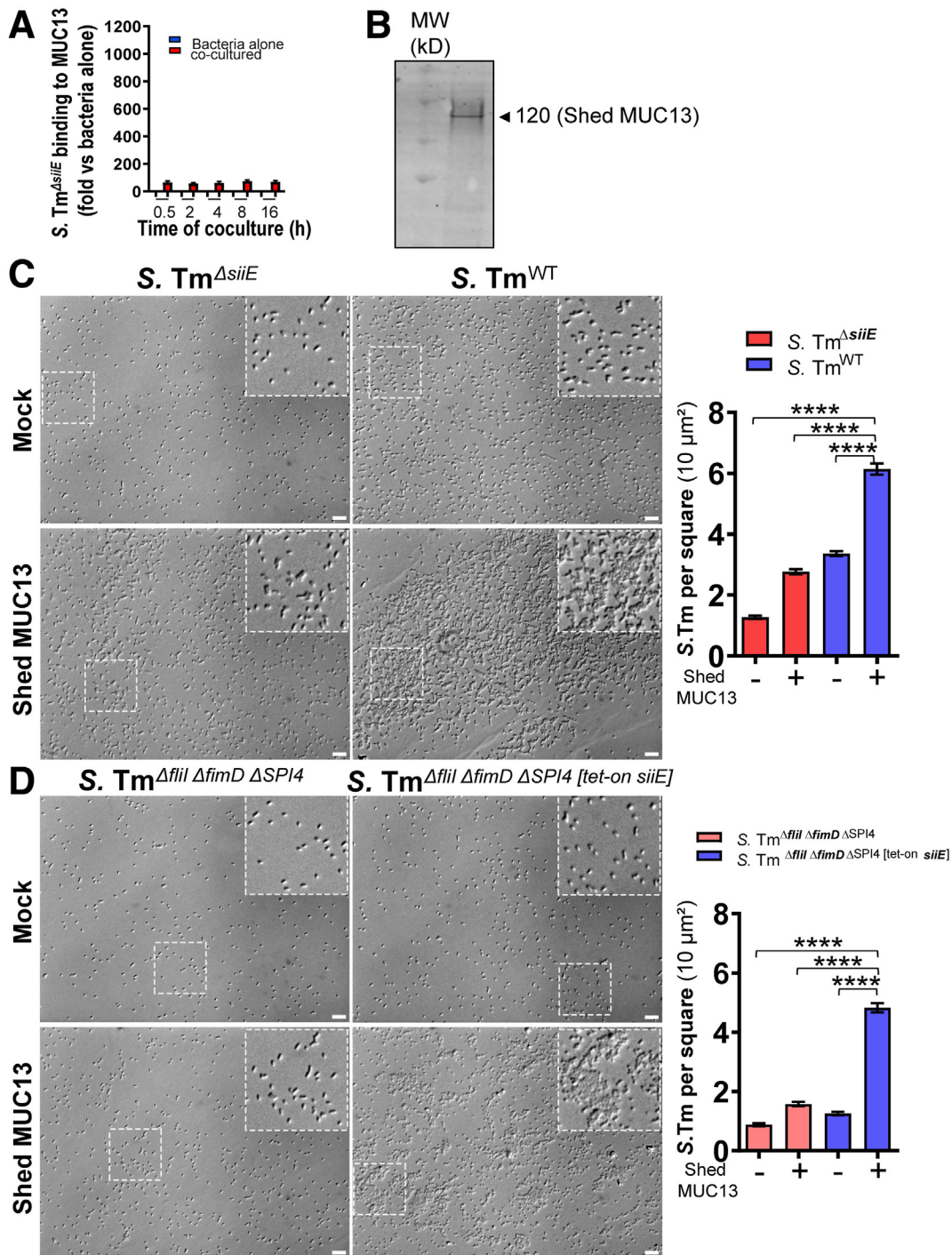


Figure 8. Specificity of MUC13 binding to SiiE. (A) In the parallel experiment described in Figure 7G and H, the presence of MUC13 on $S. Tm^{\Delta siiE}$ recovered from the conditioned medium of MUC13 expressing SW480 cells was determined by staining with the anti-FLAG antibody or an isotype control, followed by flow cytometry. (B) The gel showed purified shed MUC13 used for bacterial aggregation assay. (C) Bacterial aggregation assay with $S. Tm^{\Delta siiE}$ and $S. Tm^{WT}$ grown under SPI4-inducing conditions. *Left panel*: representative image of bacterial aggregation assay, scale bars indicate $10 \mu m$. *Right panel*: quantified by overlay image with a grid and counting of bacteria per square of $10 \mu m^2$. (D) Bacterial aggregation assays with $S. Tm$ strain MvP3078, deleted for *fil* (type I fimbriae), *filI* (flagella), and SPI4 (*siiE*), with a plasmid for inducible expression of mini-SiiE and type I secretion system, non-induced (*left*) vs induced (*right*) conditions. Representative image of bacterial aggregation assay, scale bars indicate $10 \mu m$. *Right panel*: quantified by overlay image with a grid and counting of bacteria per square of $10 \mu m^2$.

inhibited cell death in the epithelial cells through promoting nuclear factor kappa B (NF- κ B) signaling,³³ we also evaluated NF- κ B p65 (p65) level by Western blotting and

observed that the level of phosphorylation of p65 was substantially lower in the $Muc13^{-/-}$ intestine than WT intestine at 1 day of *S. Tm* infection (Figure 11B).

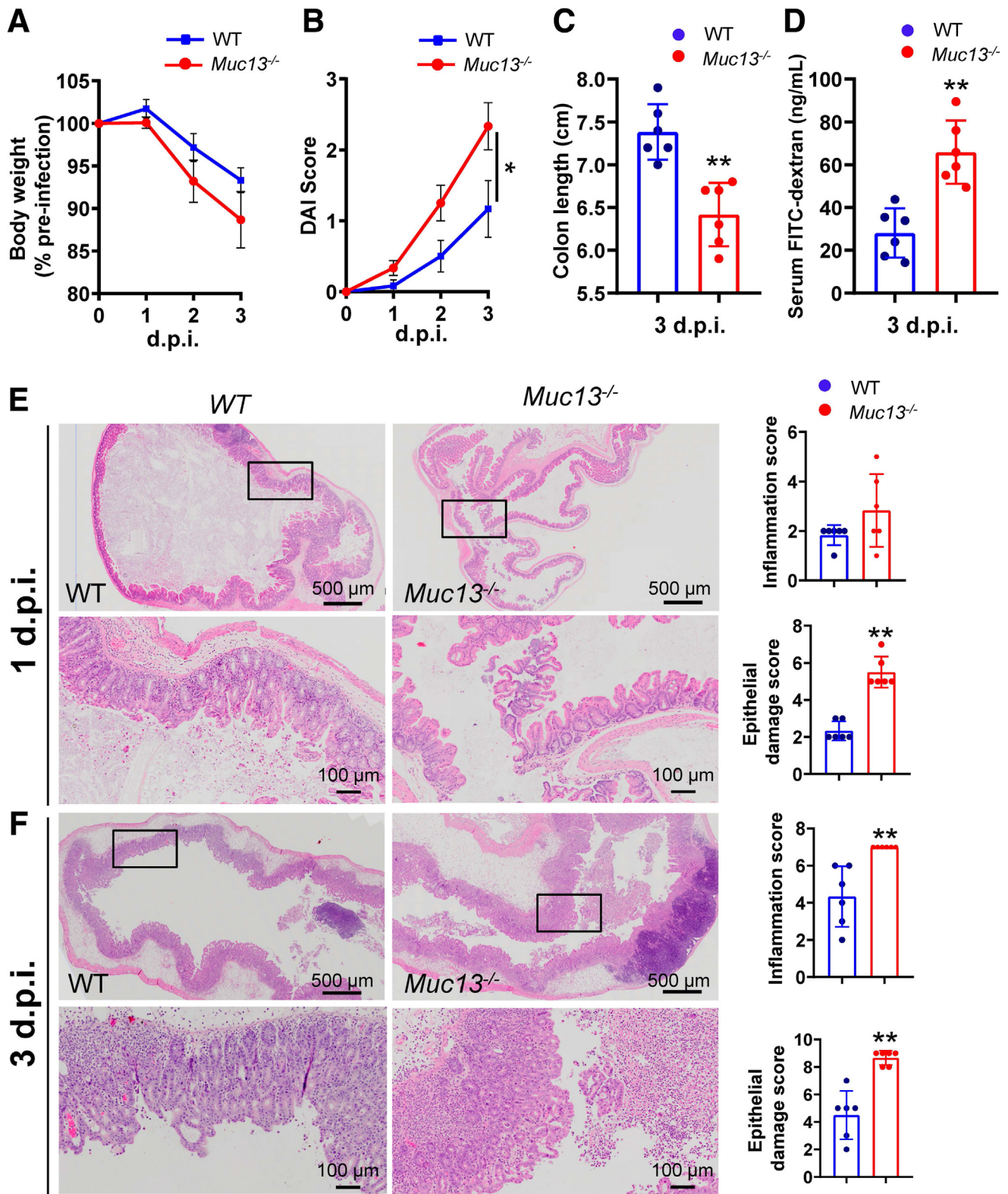


Figure 9. *Muc13*^{-/-} mice are more susceptible to *S Tm*^{AsiIE} infection. *Muc13*^{-/-} and WT littermate mice (n = 6) were infected with *S Tm*^{AsiIE} SL1344 as described in Figure 1. (A) Body weight from 0 to 3 d.p.i. expressed as percentage of pre-infected body weight. (B) Clinical DAI scores as per Figure 1 were assessed daily for 3 days. (C) Colon length at 3 d.p.i. (D) FITC-dextran intestinal permeability assay at 3 d.p.i. (E and F) H&E-stained cecal sections from representative mice infected with *S Tm*^{AsiIE} at 1 (E) and 3 (F) d.p.i., scale bars as indicated (left). Histologic scores grading severity of inflammation and tissue damage at 1 (E) and 3 (F) d.p.i. (right). Statistics: (A and B) Two-way analysis of variance with Geisser Greenhouse correction. (C–F) Individual data points, mean ± SEM, Mann-Whitney U test; *Muc13*^{-/-} vs WT mice, **P* < .05, ***P* < .01. Data are representative of 3 independent experiments.

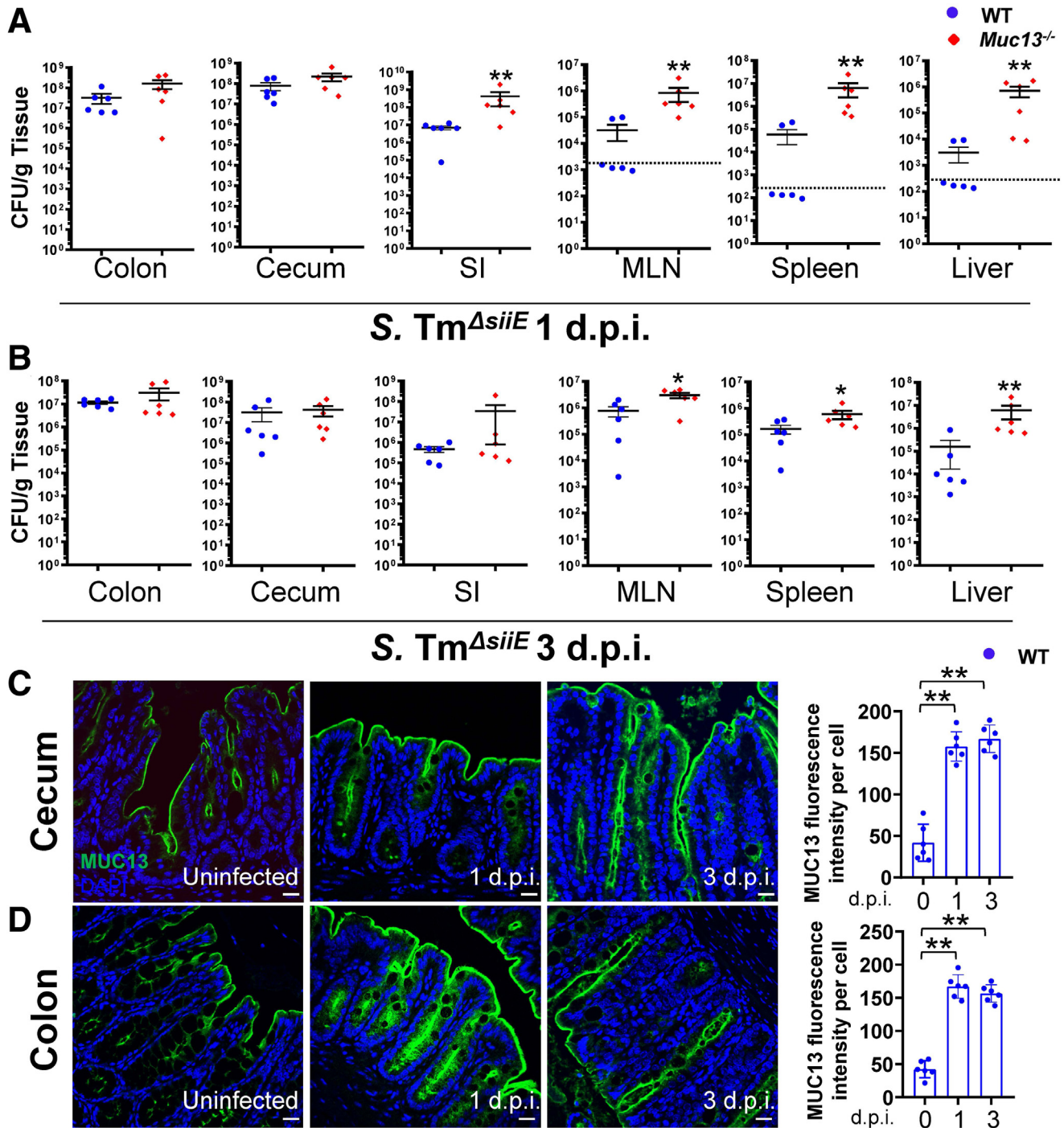


Figure 10. *Muc13*^{-/-} mice carry higher *S. Tm*^{*ΔsiiE*} burdens in MLNs, spleen, and liver. *Muc13*^{-/-} and WT littermate mice ($n = 6/\text{group}$) were infected with *S. Tm*^{*ΔsiiE*} SL1344 strain as described in Figure 1. (A and B) Concentrations of *S. Tm*^{*ΔsiiE*} in homogenates of indicated tissues were determined by limiting dilution culture 1 (A) and 3 (B) d.p.i.; dashed line, limit of detection. (C and D) Immunofluorescence staining for MUC13 (green) and nuclei (DAPI, blue) in the cecum (C) or colon (D) of WT mice. Left panel: representative immunofluorescence images; 20 μm scale bars are shown. Right panel: fluorescence intensity of MUC13 was determined by ImageJ software in at least 25 individual epithelial cells per mouse. The average intensity was plotted. Statistics: (A–D) mean \pm SEM, Mann-Whitney *U* test, $n = 6$; *Muc13*^{-/-} vs WT mice (A and B); WT mice, *1 or 3 d.p.i. vs uninfected (C and D), * $P < .05$; ** $P < .01$. Data are representative of 2 independent experiments.

Similar to infection with *S. Tm*^{WT} that induces MUC13 shedding, infection with *S. Tm*^{*ΔsiiE*}, which does not induce MUC13 shedding, also increased cell death in *Muc13*^{-/-} cecal

sections compared with WT mice. The extent of TUNEL positivity was similarly increased (typically >4-fold) in the cecum of *Muc13*^{-/-} mice compared with WT mice at both 1

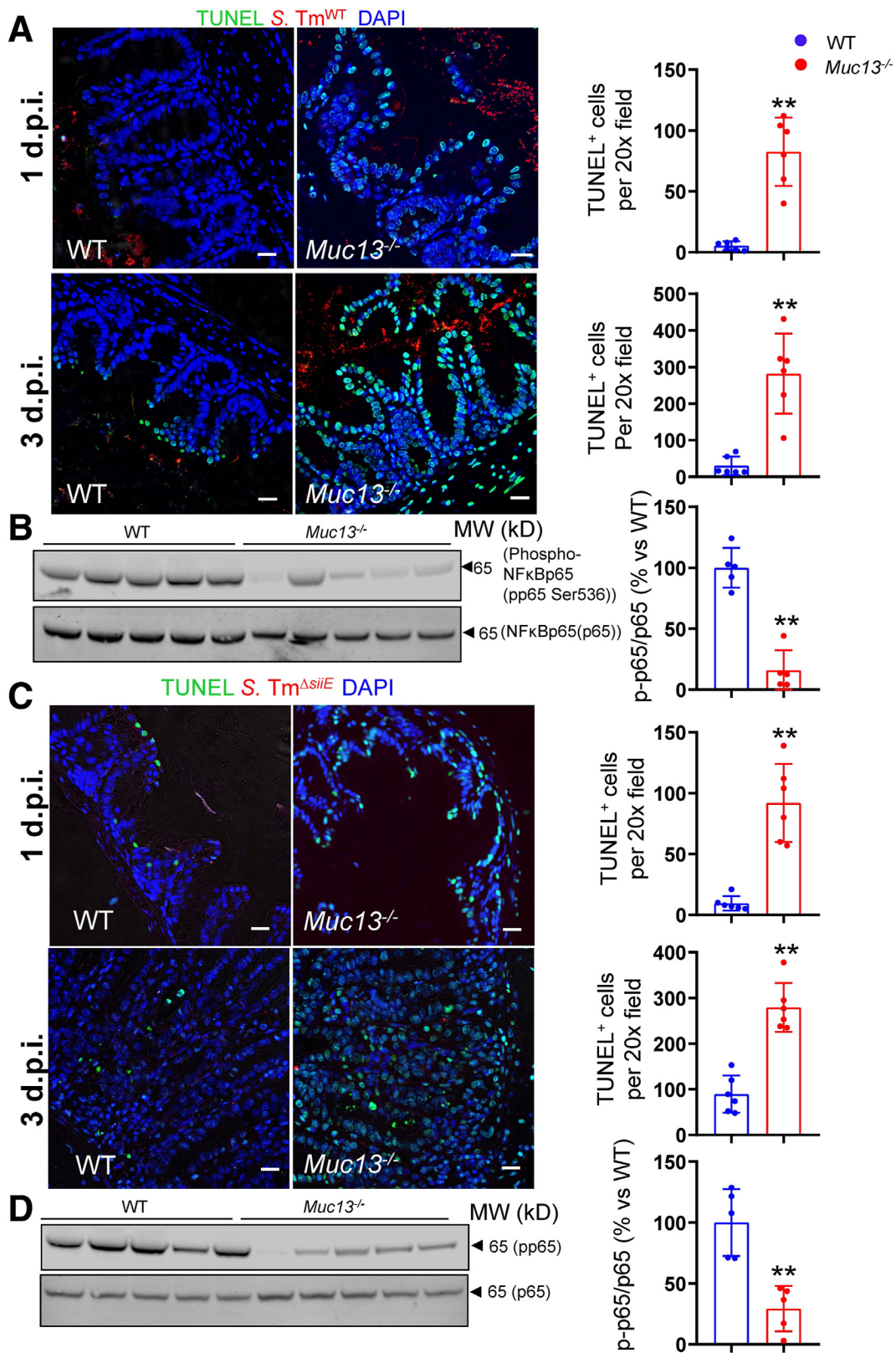


Figure 11. MUC13 inhibits intestinal epithelial cell death after both *S Tm*^{WT} and *S Tm*^{ΔsiiE} infection. *Muc13*^{-/-} and WT littermate mice ($n \geq 5$) were infected with *S Tm* SL1344 as described in Figure 1. (A and C) Left panels show representative images of cecal tissue from *Muc13*^{-/-} and WT littermate mice 1 and 3 d.p.i. with *S Tm*^{WT} (A) and with *S Tm*^{ΔsiiE} (C). Immunofluorescence staining for TUNEL (green), *S Tm* (red), and nuclei (blue). Scale bars are 20 μ m. Right panel: quantification of number of TUNEL⁺ cells per field from each mouse (average 10 independent fields). (B and D) Immunoblot analysis of phosphorylation of NF- κ B p65 (pp65) from *Muc13*^{-/-} and WT littermate mice at 1 d.p.i. with *S Tm*^{WT} (B) and with *S Tm*^{ΔsiiE} (D). Statistics: individual data points, mean \pm SEM, Mann-Whitney *U* test, *Muc13*^{-/-} vs WT mice, ***P* < .01. Data are representative of 2 independent experiments.

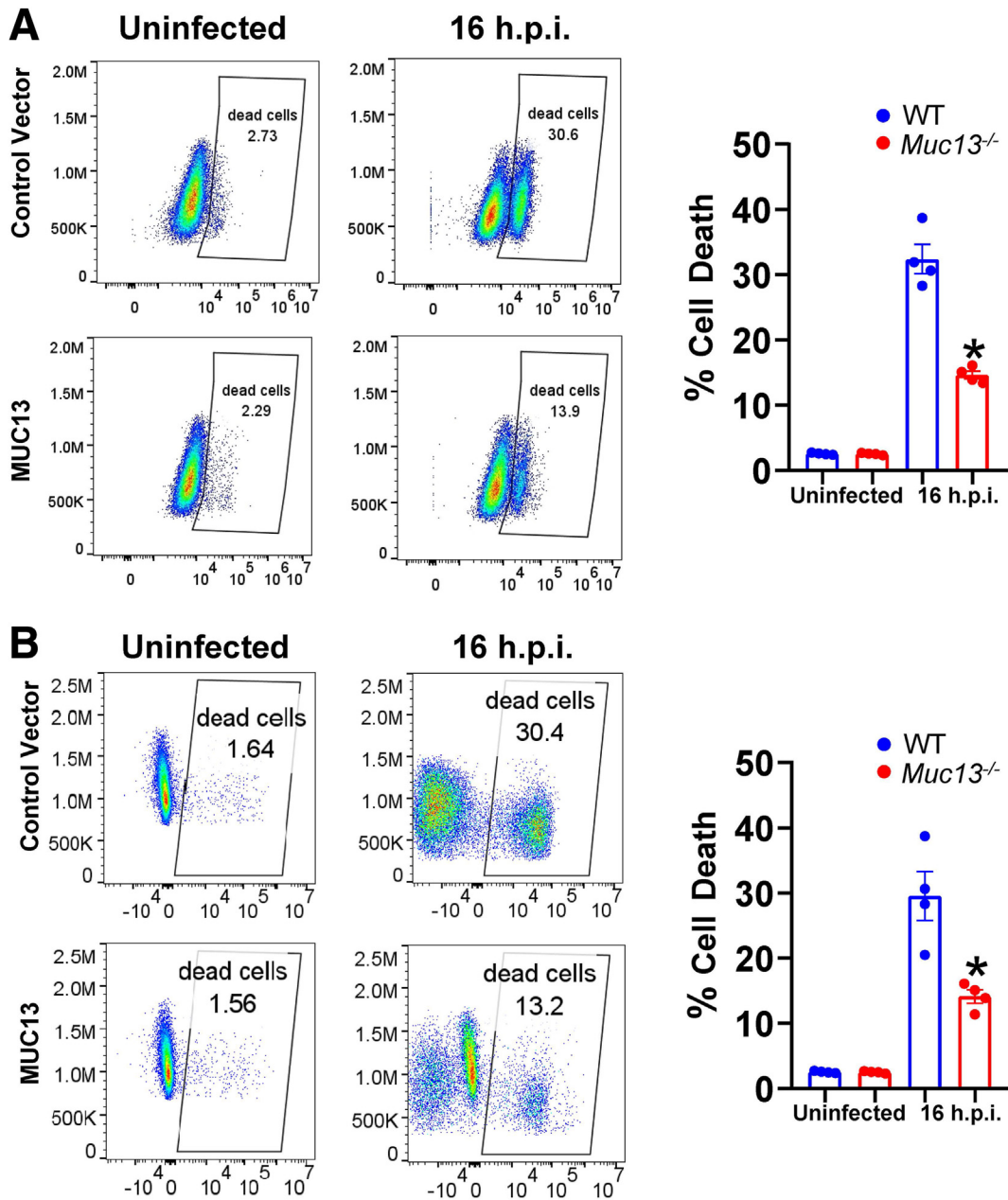


Figure 12. Expression of MUC13 in intestinal epithelial cells increases resistance to *S Tm*^{WT} and *S Tm*^{ΔsiiE} induced cell death in vitro. Vector control and MUC13 overexpressing SW480 human intestinal epithelial cells were co-cultured with *S Tm*^{WT} (A) or *S Tm*^{ΔsiiE} (B) SL1344 strain at multiplicity of infection of 1 for 16 hours. Percentage of cell death determined by flow cytometry is shown. *Left*: representative flow cytometry plots of cells stained with viability dye. *Right*: percentage of cell death was determined by flow cytometry. Statistics: individual data points, mean ± SEM, MUC13 overexpressing vs vector control SW480 cells (n = 4); *P < .05. Data are representative of 2 independent experiments.

and 3 d.p.i. (Figure 11C). We also observed decreased NF-κB phosphorylation in the *Muc13*^{-/-} ceca compared with WT 1 d.p.i. with *S Tm*^{ΔsiiE} (Figure 11D). These results were confirmed in vitro and ex vivo, where MUC13 expressing SW480 cells and cecal enteroids were protected from death after infection with both *S Tm*^{WT} and *S Tm*^{ΔsiiE}, as evidenced by ~2-fold or 4-fold decrease in numbers of dead cells in vitro or ex vivo cultures, respectively (Figures 12 and 13, Supplementary Figure 2).

Together our data suggest that MUC13 contributes to protection against *S Tm* infection in 2 ways. First, it is shed

into the lumen as a decoy receptor after engaging the pathogen, and second, via modulation of NF-κB signaling it protects epithelial cells from cell death, thus constraining infection, maintaining barrier integrity, and limiting systemic spread of pathogen.

Discussion

This is the first study providing evidence that MUC13 is an important component of intestinal mucosal defense against bacterial pathogens. In the absence of *Muc13*,

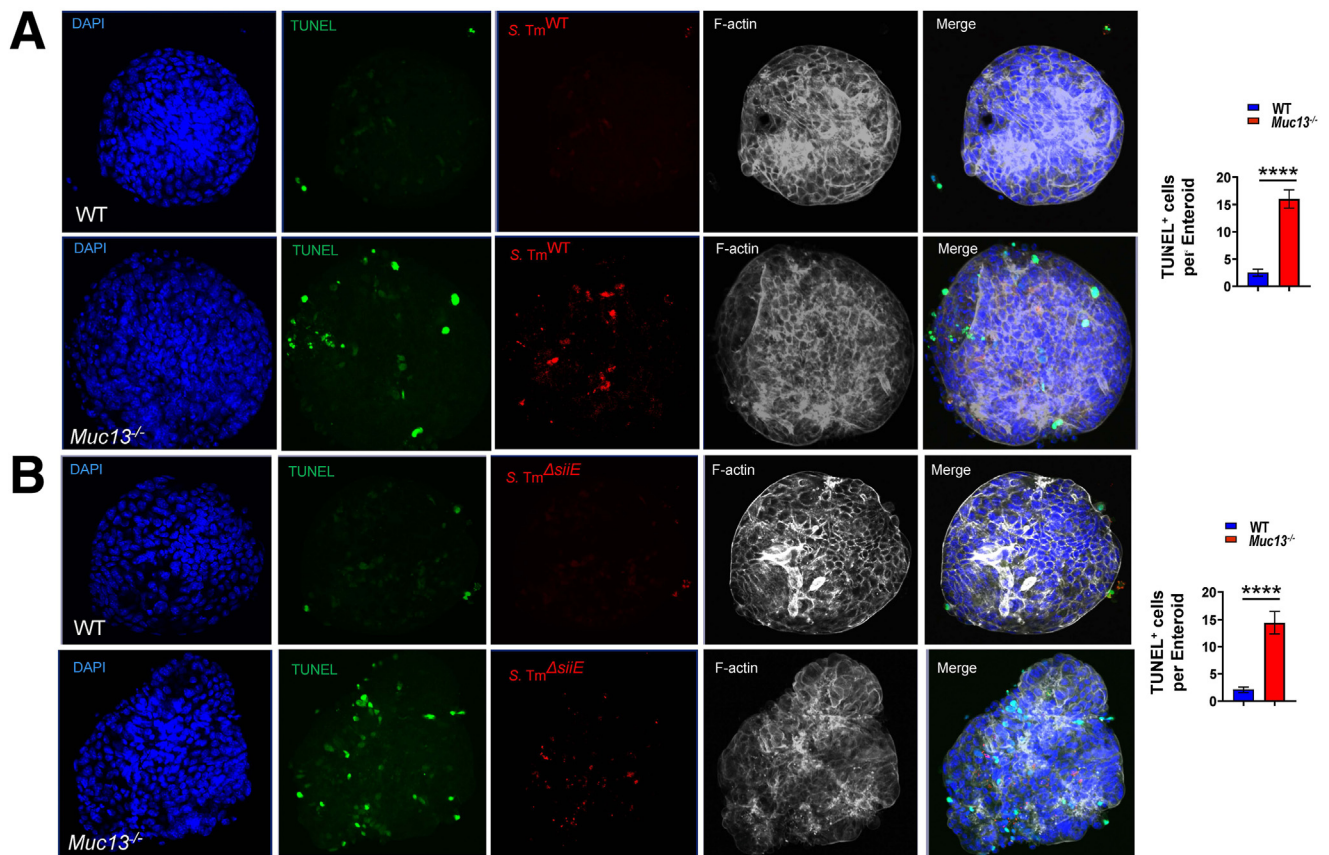


Figure 13. Enteroid expression of MUC13 increases resistance to *S Tm^{WT}* and *S Tm^{ΔsiiE}* induced cell death ex vivo. Cecal enteroids derived from *Muc13^{-/-}* mice (n = 3) or WT littermate mice (n = 3) were maintained in BME for 4 passages. Three days before infection, enteroids were transferred to suspension culture in low-attachment plates and infected with *S Tm^{WT}* DsRed (A) or *S Tm^{ΔsiiE}* mCherry (B) for 1 hour, followed by gentamicin protection assay. TUNEL-positive cells were assessed by fluorescence microscopy at 4 h.p.i. *Left panel:* representative immunofluorescence images; 20 μ m scale bars are shown. *Right panel:* results are from 20 enteroids from each genotype of 3 independent experiments. Statistics: mean \pm SEM (n = 20), Mann-Whitney U test; ****P < .0001.

Salmonella infection resulted in more severe clinical disease, higher local and systemic bacteria burden, extensive epithelial damage, and increased inflammation. Although highly expressed basally, MUC13 was rapidly up-regulated throughout the intestine in response to infection. We have demonstrated 2 mechanisms underlying this protection. First, MUC13 acts as a releasable decoy receptor after binding to *Salmonella* to limit bacterial invasion. Second, MUC13 reduces epithelial cell death, preserving barrier integrity and limiting immune infiltration. Both mechanisms limit the extent, but not the nature, of the underlying inflammatory response. Together with our previous findings with MUC1, we propose an important functional role for mucosal cell surface mucins in innate defense against bacterial pathogens.

The thick colonic mucus layer, mostly composed of the secreted mucin MUC2,²² effectively excludes the microbiota from contact with the epithelial layer and limits access to pathogens. In contrast, the cecum in mice has few goblet cells and lacks a thick continuous mucus layer. Dense mucus only fills the bottom of the crypts in the cecum, leaving the tips exposed.⁴⁹ This makes the thin layer of cell surface

mucins, like MUC13, particularly important to the defense of the cecum. The cell surface mucins family has an array of different extracellular and intracellular domains.²² Their relative expression varies along the intestinal tract and between different cell types within each region.²² Their expression levels rapidly adjust to environmental cues to limit microbial infection and modulate inflammatory responses at the environment interface.²² MUC1 has already been shown to limit infection by a wide variety of pathogens and to regulate inflammatory responses to infection.^{26,27,53}

However, the role of other cell surface mucins in infection remains largely unexplored, and it is not clear what level of redundancy exists given the colon expresses cell surface MUC1, 3, 4, 12, 13, and 17. We observe a compensatory increase in the expression of *Muc1* at late time points in the absence of *Muc13* in response to the *S Tm* infection. Despite this increase, *Muc13^{-/-}* mice remained extremely susceptible to infection, suggesting a non-redundant role for MUC13 in protection against *Salmonella*.

The shedding of cell surface mucins, including MUC13, remains a relatively unexplored area of research. In contrast, the release of MUC1, a well-studied cell surface

mucin, is mediated through non-covalent interactions between the α - and β -subunits, which are dissociated by cell surface proteases^{54,55} and shear forces after binding to highly motile bacterial.²⁸ Although lacking a canonical cleavage site, MUC13 exhibits several SEA domain features³² and has been found to undergo cleavage within this domain based on biochemical analyses.^{32,36} Furthermore, proteomic analyses have established MUC13 as a significant component of secreted mucus.^{37,38} Further studies are needed to identify the specific amino acid sequence required for MUC13 cleavage.

MUC1 has also been shown to act as a receptor for the *S Tm* SiiE adhesion, which enables apical invasion into intestinal epithelial cells. However, these findings are limited to in vitro experiments using cancer cell lines²⁹ and have not been shown to result in increased infection in vivo.²⁶ We also observed that *S Tm* binds to the extracellular domain of MUC13 through its giant SiiE adhesin. Furthermore, we showed that MUC13 acts as a pathogen-binding decoy shed from the epithelial cell surface after the binding, limiting the successful adhesion of *S Tm* to the cell surface and subsequent invasion from both in vivo and in vitro data. The difference in the *S Tm* invasion mediated by the 2 cell surface mucins could be due to (1) different cell surface mucins and (2) different cell lines in vitro experiments. It is important to note that MUC13 is much more highly expressed than MUC1 in the intestine.²²

Moreover, we observed focal binding of MUC13 to *S Tm* (Figure 7E). Focal binding would prevent adhesion to the glycocalyx, and shedding of MUC13 would detach the bacteria. The success of this form of host defense will be stochastic. Despite high levels of MUC13, some bacteria will still successfully adhere to and invade the cecal epithelium. However, it is plausible that this defense, continuously used, limits infectious events, leading to reduced infectious burden, and may distinguish symptomatic from asymptomatic infection, particularly with low-dose exposures to pathogens.

On the basis of our results and the structure and cellular localization of MUC13 in the luminal glycocalyx, we propose that MUC13 acts at 2 distinct levels in defense against pathogens. First, luminal engagement of the extracellular domain of MUC13 induces its shedding and releasable decoy activity. This limits prolonged adherence and invasion and is dependent on bacterial SiiE adhesin expression. During this process, *S Tm* is coated with MUC13. We propose that this may further limit adhesion to epithelia by blocking this key adhesin. It reduces the frequency of contact between *S Tm* and epithelial cells, thus reducing translocation of T3SS-1 effector proteins, which results in less activation of host proinflammatory responses. We further demonstrated that shed MUC13 specifically bound to *S Tm* through SiiE adhesin and not other surface structures (Figure 8C and D).

The second level of host defense induced by MUC13 is through inhibition of cell death, which preserves barrier integrity under stress. In several previous studies, we have illustrated that cytoplasmic MUC13 translocates to the nucleus, where it cooperates with NF- κ B to suppress cell death in response to a wide range of cellular stresses and chemical

insults.^{25,33,34} The importance of the pro-survival activity of MUC13 explains why both the MUC13 binding (*S Tm*^{WT}) and non-MUC13 binding (*S Tm* ^{Δ SiiE}) bacteria induce greater pathology in *Muc13*^{-/-} mice despite the loss of the cell surface decoy function. In both ex vivo and in vitro, infection of MUC13-expressing cells with either *S Tm*^{WT} or *S Tm* ^{Δ SiiE} prevents epithelial cell death by $\geq 50\%$ compared with the cells lacking *MUC13* expression (Figures 12 and 13). This indicates that epithelial cell death is limited by MUC13 in response to infection. Studies of *-Salmonella*-infected HeLa, HCT116, and Caco2 BBE cells showed that the bacterial SPI1 effector protein AvrA can inhibit pro-survival NF- κ B signaling.^{56–58} Because we observed increased bacterial burden in *Muc13*^{-/-} ceca, this also explains why we observe less NF- κ B activation in *Muc13*^{-/-} than WT. MUC13 also blocks β -catenin degradation, increasing its cytoplasmic and nuclear levels inhibiting cell death and increasing proliferation.⁵⁹ In addition to a possible effect on NF- κ B, we have also shown that MUC13 can promote responses to PAMPs mediated by TLRs.³⁴ Consequently, in addition to limiting bacterial attachment to the cell surface, MUC13 also modulates inflammatory and cell death responses during infection.

We have previously published that MUC13 protects against DSS-induced intestinal inflammation by inhibiting epithelial cell apoptosis.²⁵ In line with this finding, we now demonstrate that MUC13 also protects from cell death in response to infection. Epithelial cell shedding of infected cells is an effective host defense mechanism at the early stage of infection.⁶⁰ However, the widespread *S Tm*-induced epithelial cell death we observed in our experiments, particularly in the absence of MUC13, allows the bacteria to breach the epithelial barrier, access the underlying tissues, and establish systemic infection.²⁰ This also provided an enriched nutrient source for the large expansion of *S Tm* observed in the *Muc13*^{-/-} ceca. It is worth noting that large numbers of *S Tm* were observed in sheets of shed epithelial cells in the lumen of *Muc13*^{-/-} ceca. Thus, appropriate expression and function of MUC13, and likely the entire family of cell surface mucins, limit the severity of mucosal bacterial infection.

In conclusion, we demonstrate for the first time that MUC13 is a critical element against *S Tm* infection. MUC13 acts as a pathogen-binding decoy and inhibits cell death. Polymorphisms in MUC13 and other mucins may predispose individuals to both acute infection and chronic inflammatory disease.

Materials and Methods

Ethics Statement

All mouse experiments, maintenance, and care were performed in accordance with the Australian Code for the Care and Use of Animals for Scientific Purposes 8th edition (2013) and were approved by The University of Queensland Animal Experimentation Ethics Committee.

Mice

Muc13^{+/+}(WT) and *Muc13*^{-/-} mice²⁵ fully backcrossed onto a C57BL/6 background were bred within

a specific pathogen-free animal facility at the Translational Research Institute. Mice were litter mates that were sex- and age-matched within experiments (6–12 weeks of age).

In Vivo S Tm Infection

The naturally streptomycin-resistant *S Tm* SL1344 strain or *S Tm* NCTC 12023 strain or *S Tm*^{Δ*stiiE*} SL1344 strain was grown overnight at 37°C in LB broth supplemented with kanamycin or ampicillin, subsequently diluted 1:100, and cultured under aeration until OD₆₀₀ = 0.4. Bacteria were washed twice in cold phosphate-buffered saline (PBS) and resuspended at 4 × 10⁷ CFU per 100 μL. The *S Tm* strain used in this study has been engineered to express LUX (kanamycin resistant), DsRed (ampicillin resistant), or mCherry (ampicillin resistant). For oral infection, mice were gavaged orally with streptomycin (20 mg/mice) 24 hours before infection, then orally gavaged with 4 × 10⁷ CFU *S Tm*, and euthanized at 1 or 3 d.p.i. Gastrointestinal tract organs (cecum, colon, and small intestine) and systemic organs (MLNs, spleen, and liver) were dissected and collected in PBS, fixed in 10% formalin, or frozen. To assess the number of CFU/g tissue, the tissue was rinsed through 5 Petri dishes containing PBS in sequence. This was done to eliminate any luminal contents and attached mucus before the tissue was homogenized in 0.1% Triton X-100 in serially diluted, plated onto selective agar plates, and incubated at 37°C overnight. Colonies were then counted and normalized to tissue weights.

Bioluminescence Imaging

Mouse intestines were harvested and imaged for bioluminescence using an IVIS Spectrum system (PerkinElmer, Glen Waverley, Australia). Images were processed and compared, and total bioluminescence fluxes were quantified using IVIS Living Image Software (PerkinElmer).

Assessment of Clinical Scores

Body weight, stool scores, and behavior/activity were assessed daily. Scoring for stool consistency and occult blood was adapted as described previously.⁶¹ In brief, stool scores were determined as follows: 0, well-formed pellets; 1, semi-formed stools; 2, soft stools; 3, liquid stools that adhered to the anus. Weight loss scores were determined as follows: 0, less than 5% weight loss; 1, 5%–14% weight loss; 2, 15%–19% weight loss; 3, more than 20% weight loss. Inactivity scores were determined as follows: 0, normal; 1, fully mobile but more inactive than usual; 2, mouse moving only occasionally but responsive to prompting; 3, mouse moving only occasionally and largely unresponsive to prompting. Shivering and Ruffled fur scores were determined as follows: 0, normal; 1, occasional shivering; 2, mouse noticeably shivering with some restricted ruffling of fur; 3, constant prominent shivering with obvious ruffling of most fur. Hunched posture scores were determined as follows: 0, normal; 1, small change in normal posture; 2, mouse noticeably hunched over and could regain

normal posture; 3, mouse noticeably hunched over without regaining normal posture.

Assessment of Epithelial Damage, Tissue Inflammation, and Intestinal Permeability

Excised ceca were fixed using 10% (v/v) formalin in PBS and embedded in paraffin, and 4-μm sections were stained with H&E. Histologic assessment of cecum mucosae was carried out in a blinded fashion using a protocol as described previously (Table 1).^{47,61} To assess intestinal permeability, mice were gavaged orally with 4 kDa FITC-dextran (Sigma, 400 mg/kg body weight in PBS), blood samples were obtained at 2 hours, and plasma FITC-dextran concentrations were determined by measuring fluorescence at 520 nm emitted in a 96-well plate excited with 474 nm laser using PHERAstar versus FITC-dextran standard curve (BMG Labtech, Victoria, Australia).

Confocal Microscopy

Cecum paraffin sections (4 μmol/L) were affixed to adhesive slides and air-dried overnight at 37°C. After dewaxing in xylol and rehydration through descending graduated ethanol, sections were antigen-retrieved by heating for 20 minutes in 10 mmol/L citric acid (pH 6) and cooled to room temperature. Sections were permeabilized (PBS/0.5% Triton X-100) and blocked (PBS/10% Normal Goat Serum). Antibody staining included rabbit anti-MUC13 antibody,⁶² anti-MUC2C3 antisera (from Prof Gunnar Hansson), anti-*S Tm* LPS (Santa Cruz Biotechnology, Inc, Dallas, TX), chicken anti-rabbit IgG (H+L) Cross-Adsorbed Secondary Antibody, Alexa Fluor 488 (Invitrogen, cat #A21441), and goat anti-mouse IgG (H+L) Highly Cross-Adsorbed Secondary Antibody, Alexa Fluor 546 (Invitrogen, cat #A 11030) secondary reagents, and DAPI (Sigma-Aldrich, St Louis, MO).

RNA Preparation and Real-Time Polymerase Chain Reaction

Total RNA was prepared using the RNeasy Mini Kit (Qiagen, Valencia, CA). The quantity of the RNA was determined by spectrophotometry (ND-1000; NanoDrop Technologies Inc, Wilmington, DE). Total RNA (1 μg) from each sample was used for first-strand cDNA synthesis using SuperScript III reverse transcriptase (Invitrogen) following the manufacturer's instructions. Depending on the targeted genes, the cDNA was diluted up to a 1:10 ratio to perform polymerase chain reaction. The 2.5 μL of diluted cDNA, 0.75 μL of 2 μmol/L desired primer, 3.75 μL of SYBR green (SensiFAST SYBR Lo-ROX kit; Biorline), and 0.5 μL of DNase and RNase free water were mixed and run in a Real-Time PCR System (Applied Biosystems ViiA 7; Life Technologies Corporation, Carlsbad, CA) for 40 cycles. The Ct values were then analyzed using ViiA 7 software (Life Technologies Corporation). To confirm the specificity of the amplified DNA, a melting curve was determined at the end of each run. The reaction efficiency was determined with a dilution series of cDNA containing the polymerase chain reaction products. Genes were normalized to the unregulated

Table 1. Histologic Scoring System for *S Tm*-Induced Colitis

Feature	Score	Description
Inflammation severity	0	None
	1	Mild
	2	Moderate
	3	Severe
Inflammation extent	0	None
	1	Infiltrate around the crypt base
	2	Infiltrate reaching to muscularis mucosae
	3	Extensive infiltrate reaching to muscularis mucosae and thickening of the mucosa with abundant edema
	4	Infiltrate reaching to submucosae
Epithelial damage	0	None
	1	Some loss of goblet cells/some crypt abscesses or damage
	2	Loss of goblet cells in large areas/extensive crypt abscesses or damage
	3	Loss of crypts <5 crypt widths
	4	Loss of crypts >5 crypt widths, <20% ulceration
	5	≥20% ulceration
Percentage involvement of epithelial damage	0	0%
	1	1%–25%
	2	26%–50%
	3	51%–75%
	4	76%–100%

housekeeping gene *Hprt* or *villin 1*, and the results were expressed as the ratio of the target gene and housekeeping gene expression (arbitrary units). Control experiments were also performed to ensure that housekeeping gene expression was not differentially regulated under the experimental conditions used. Primers used for polymerase chain reaction were designed from Primer Bank (<http://pga.mgh.harvard.edu/primebank/index.html>) or using Oligoperfect Designer (Life Technologies), and their sequences to amplify the target genes are shown in Table 2.

Crypt Isolation and Enteroids Culture

Crypts were isolated from the cecum of WT and *Muc13*^{-/-} mice as described.⁶³ Briefly, the cecum was opened

longitudinally, washed in PBS, and cut into 5-mm pieces. The tissue pieces were incubated in 10 mmol/L dithiothreitol in PBS for 5 minutes at room temperature and then transferred the pieces to 8 mmol/L EDTA in PBS with continuous rotation slowly at 4°C for 30 minutes. We replaced the supernatant with PBS and shook vigorously; this will yield a supernatant enriched in crypts. The isolated crypts were washed with Advanced DMEM/F12 medium and centrifuged at 50g for 5 minutes at 4°C. The pellets were then suspended in Matrigel (BD Matrigel, Basement Membrane Matrix [BME]) at 10–40 crypts/μL and plated in 24-well (20 μL/well) plates, cultured in Advanced DMEM/F12 + 50% L-WRN conditioned medium + 10 μmol/L Y-27632 (ROCK inhibitor; Tocris Bioscience and R&D Systems,

Table 2. Primer Set for Quantitative Polymerase Chain Reaction to Detect the Indicated mRNA Levels

	Forward primers	Reverse primers
<i>Hprt</i>	5'-ATTAGCGATGATGAACCAGGTTATG-3'	5'-AGCAAGTCTTTCAGTCCTGTCCA-3'
<i>Ii22</i>	5'-GCTCAGCTCCTGTACATCA-3'	5'-CAGTTCCTCAATCGCCTTGA-3'
<i>Cxcl10</i>	5'-TCCTTGCTCCTCCCTAGCTCA-3'	5'-ATAACCCCTTGGGAAGATGG-3'
<i>Cxcr2</i>	5'-GCCCTGCCATCTTAATTCTAC-3'	5'-ACCCTCAAACGGGATGTATTG-3'
<i>Lcn2</i>	5'-ACATTTGTTCCAAGCTCCAGGGC-3'	5'-ACATTTGTTCCAAGCTCCAGGGC-3'
<i>Reg3g</i>	5'-ATGGCTCCTATTGCTATGCC-3'	5'-GATGCTCCTGAGGGCCTCTT-3'
<i>S100a8</i>	5'-TGTCCTCAGTTTGTGAGAATATAAA-3'	5'-TCACCATCGCAAGGAAGTCC-3'
<i>S100a9</i>	5'-GGTGAAGCACAGTTGGCA-3'	5'-GTGTCCAGGTCCTCCATGATG-3'
<i>β-defensin</i>	5'-GCATTGGCAACACTCGTCAG-3'	5'-GTTTAACGGGATCTTGGTCTTCT-3'
<i>Villin</i>	5'-CTGGCTTGGGATCCCTCAA-3'	5'-TCGGGCTCATAACCTCGTCA-3'
<i>Muc1</i>	5'-CCCTATGAGGAGGTTTCGGC-3'	5'-GTGGGGTGACTTGCTCCTAC-3'
<i>Muc2</i>	5'-CCATTGAGTTTGGGAACATGC-3'	5'-TTCGGCTCGGTGTTTCAGAG-3'
<i>Muc13</i>	5'-GCCAGTCTCCACCACGGTA-3'	5'-CTGGGACCTGTGCTTCCACCG-3'

Minneapolis, MN) + 10 $\mu\text{mol/L}$ SB 202190, and medium was changed every 3–4 days. The enteroids were cultured and allowed to grow in BME for at least 4 passages to ensure no leukocytes are present in the culture. Enteroid growth was monitored by light microscopy. Enteroid suspension culture was performed as described.⁵⁰ Two-dimensional monolayer Transwell culture was performed as described with slight modifications.^{64,65} Briefly, to form a two-dimensional enteroid monolayer, Transwell filters (cat #3413; Corning Costar, Tewksbury, MA) were coated with collagen IV solution at a final concentration of 10 $\mu\text{g}/\text{cm}^2$ and incubated at 37°C for ≥ 2 hours. The enteroids were extracted from BME by first washing in a solution of 0.5 mmol/L EDTA and then dissociated for 5 minutes at 37°C using a solution of 0.05% trypsin/0.5 mmol/L EDTA. The trypsin was then inactivated using Advanced DMEM/F12 + 10% fetal bovine serum. The enteroids were dissociated by pipetting. The cells were then passed through a 40 μm cell strainer (BD Biosciences) and resuspended in 50% L-WRN conditioned medium + 10 $\mu\text{mol/L}$ Y-27632. On average, enteroids from 3 wells of a 24-well plate were plated into one Transwell filter in 100 μL of medium. The confluency of monolayers was determined by transepithelial electrical resistance measured.

Generating N-terminal FLAG-Tagged MUC13 Overexpression Stable Clones in SW480 Cell Line (5FLAGMUC13 SW480)

The FLAG tag and restriction sites were introduced by polymerase chain reaction using Pfu Ultra (Agilent) High-Fidelity DNA polymerase, and the primers sequence are listed in Table 3. The FLAG-MUC13 fragments were amplified from human MUC13 cDNA and cloned into the retroviral vector pRUF. The identity of the cloned sequences was verified by DNA sequencing equivalent to human MUC13 (GenBank accession no. AF286113) (Australian Genomic Research Facility (St Lucia, Australia).

Five $\times 10^6$ amphotropic (PA317) packaging cells were transfected with 10 μg DNA of the appropriate retroviral construct (pRUFneo) by Lipofectamine 2000 Reagent (Life Technologies) according to the manufacturer's protocol. Culture supernatants were collected 36–48 hours after transfection and filtered through a 0.45 μm filter. SW480 cells were infected with the filtered viral supernatants in the presence of 4 $\mu\text{g}/\text{mL}$ polybrene (Sigma-Aldrich) for 12 hours, after which the medium was changed. Fresh viral suspensions were added after 24-hour interval for an additional 12 hours. Infected cells were selected for 5 days in 100 $\mu\text{g}/\text{mL}$ G418.

Assessment of MUC13 Binding to *S Tm* by Flow Cytometry

For MUC13 detection, co-culture 5FLAGMUC13 SW480 cells were harvested with trypsin and stained with BD Horizon fixable viability stain 575V dye (BD) either stained without fixation (staining of cell surface structures) or fixed in 1% paraformaldehyde for 5 minutes on ice and then permeabilized with 0.5% saponin (intracellular and

Table 3. Primer Set for Generating FLAG-MUC13 Construct

Forward primer with <i>Bam</i> HI restriction enzyme	5'- TGG ATC C ATG AAA GCC ATC A TT CAT CTT ACT CTT CTT GCT CTC CTT TCT GTA AAC ACA GCC GAT TAC AAG GAT GAC GAT GAC AAG ACC AAC CAA GGC AAC -3'
Reverse primer with <i>Hind</i> III restriction enzyme	5'- GAA GCT T CTA ATA GTC AGG GCG GGG CAT -3'

extracellular staining). The cells were then incubated with the anti-FLAG antibody (Sigma-Aldrich) or isotype control 401.21 at 10 $\mu\text{g}/\text{mL}$ in 1% bovine serum albumin in PBS for 60 minutes at 4°C and then with anti-mouse antibody conjugated to FITC (Invitrogen). For the detection of intracellular antigens, washes, and antibody incubations were performed in the presence of 0.5% saponin. After staining, all cells were fixed with 1% paraformaldehyde. The analysis was gated on viable cells, and assessment of staining was performed on a CytoFLEX flow cytometry (Beckman Coulter, Brea, CA) using the Flowjo v10 software (Flowjo, LLC, Ashland, OR). Bacteria were recovered from the culture medium of SW480 cells by first sedimenting non-adherent mammalian cells (300g, 5 minutes) and then sedimenting bacteria (10,000g, 10 minutes). Bacteria were then stained with anti-FLAG antibody or 401.21 at 10 $\mu\text{g}/\text{mL}$ as above and gated using the SSC and FSC pattern of broth cultured *S Tm*.

Assessment of MUC13 Binding to *S Tm* by Confocal Microscopy

Bacteria prepared and stained for flow cytometry as above were smeared onto charged glass slides, stained with DAPI (0.1 $\mu\text{g}/\text{mL}$) for 15 minutes, washed with PBS, mounted in Prolong Gold (Invitrogen), and examined using an Olympus FV1200 confocal microscope with multitracking detecting DAPI (excitation 405nm, detection 420–480 nm) and FITC (excitation 488 nm detection, LP 505 nm) fluorescence separately.

Gentamicin Protection Assays

A confluent layer of SW480 cells was prepared by seeding 5×10^4 cells per well in 96-well cell culture plates. For the invasion assay, an overnight culture of bioluminescent *S Tm* SL1344 was diluted 1:100 and cultured under aeration until OD600 = 0.4. Bacteria were diluted 1:40 in RPMI1640 (approximately 10^6 CFU/mL), and bacteria were added to yield a multiplicity of infection of 1:1. Cells were washed twice with PBS and once with fresh prewarmed medium (RPMI 1640 with 10% fetal calf serum) before inoculation. Plates were centrifuged for 1 minute at 500g and incubated in culture medium at 37°C in 5% CO₂ for 30 minutes, and then inoculums were removed, and plates were washed with PBS 5 times and incubated in culture medium containing 50 $\mu\text{g}/\text{mL}$ gentamicin for 1 hour. Cells were then washed twice with PBS, and a culture medium

containing 20 $\mu\text{g}/\text{mL}$ gentamicin was added. At this point, the initial luminescent readings were taken. Bioluminescent readings were taken at the indicated time points.

Bacterial Aggregation Assay

WT *S Tm* and isogenic strains MvP493 ($\Delta\text{SPI4}::\text{aph}$), MvP599 ($\Delta\text{siiE}::\text{FRT}$), MvP3078 ($\Delta\text{flil}::\text{FRT}$ $\Delta\text{fimD}::\text{FRT}$ $\Delta\text{SPI4}::\text{FRT}$) were used to test mucin-induced cell aggregation. Overnight cultures of *S Tm* strains were diluted 1:31 in fresh LB broth and subcultured for 2.5 hours at 37°C with aeration. *S Tm* strains with plasmid p4906 for overexpression of *hilD* regulator or plasmid p5714 harboring the *sii* operon with a mutant form of *siiE* under control of the *tetR* P_{tetA} cassettes were cultured for 1 hour without the non-antibiotic tetracycline derivative anhydrotetracycline and further incubated for 1.5 hours with 10 ng/mL anhydrotetracycline. Bacterial cultures were diluted to OD 0.1 and centrifuged for 5 minutes at 4000g. Cell pellets were resuspended in HEPES buffer with or without the addition of mucins as indicated and incubated for 1 hour at room temperature. Next, 5 μL of the suspensions was spotted onto agarose pads on microscope slides. Bacteria were visualized by brightfield microscopy using a Zeiss Cell Observer microscope with DIC illumination. Bacteria were quantified by overlay image with a grid and counting of bacteria per square of 10 μm^2 .

Assessment of Intestinal Cell Death

Dying cells in tissue sections were detected using TUNEL with a fluorescein staining (In Situ Cell Death Detection Kit, Roche Diagnostic) according to the manufacturer's instructions. Nuclei were stained with DAPI (0.1 $\mu\text{g}/\text{mL}$), and sections were washed with PBS, mounted in Prolong Gold (Invitrogen), and examined using an Olympus FV1200 confocal microscope with multitracking detecting DAPI (excitation 405 nm, detection 420–480 nm) and FITC (excitation 488 nm detection, LP 505 nm) fluorescence separately. The number of positive-staining cells was counted per field (20 μm).

In Vitro Cell Death Assay

MUC13 overexpressed or vector control SW480 cells were treated with *S Tm* for 16 hours, and then the cells were harvested. Cell viability was analyzed by flow cytometry on cells stained with BD Horizon fixable viability stain 575V dye (BD) following the manufacturer's instructions and analyzed by CytoFLEX flow cytometry (Beckman Coulter, Brea, CA) using the Flowjo v10 software.

Statistical Analysis

Because of difficulties in verifying the normality of distributions when the sample size is small, we have taken a conservative approach and used the nonparametric Mann-Whitney *U* test. All statistical analyses were performed using Prism v8 (GraphPad Software, San Diego, CA). The statistical test used and the sample sizes for individual analyses are provided within the figure legends.

References

1. Majowicz SE, Musto J, Scallan E, et al. The global burden of nontyphoidal Salmonella gastroenteritis. *Clin Infect Dis* 2010;50:882–889.
2. Ochman H, Soncini FC, Solomon F, et al. Identification of a pathogenicity island required for Salmonella survival in host cells. *Proc Natl Acad Sci U S A* 1996;93:7800–7804.
3. Collazo CM, Galan JE. The invasion-associated type III system of Salmonella typhimurium directs the translocation of Sip proteins into the host cell. *Mol Microbiol* 1997;24:747–756.
4. Shea JE, Hensel M, Gleeson C, et al. Identification of a virulence locus encoding a second type III secretion system in Salmonella typhimurium. *Proc Natl Acad Sci U S A* 1996;93:2593–2597.
5. Kubori T, Matsushima Y, Nakamura D, et al. Supramolecular structure of the Salmonella typhimurium type III protein secretion system. *Science* 1998;280:602–605.
6. Zhou D, Mooseker MS, Galan JE. An invasion-associated Salmonella protein modulates the actin-bundling activity of plastin. *Proc Natl Acad Sci U S A* 1999;96:10176–10181.
7. Zhou D, Mooseker MS, Galan JE. Role of the *S. typhimurium* actin-binding protein SipA in bacterial internalization. *Science* 1999;283:2092–2095.
8. Hardt WD, Chen LM, Schuebel KE, et al. *S. typhimurium* encodes an activator of Rho GTPases that induces membrane ruffling and nuclear responses in host cells. *Cell* 1998;93:815–826.
9. Carlson SA, Jones BD. Inhibition of Salmonella typhimurium invasion by host cell expression of secreted bacterial invasion proteins. *Infect Immun* 1998;66:5295–5300.
10. Velge P, Wiedemann A, Rosselin M, et al. Multiplicity of Salmonella entry mechanisms, a new paradigm for Salmonella pathogenesis. *Microbiologyopen* 2012;1:243–258.
11. Soto GE, Hultgren SJ. Bacterial adhesins: common themes and variations in architecture and assembly. *J Bacteriol* 1999;181:1059–1071.
12. Wagner C, Hensel M. Adhesive mechanisms of Salmonella enterica. *Adv Exp Med Biol* 2011;715:17–34.
13. Wagner C, Barlag B, Gerlach RG, et al. The Salmonella enterica giant adhesin SiiE binds to polarized epithelial cells in a lectin-like manner. *Cell Microbiol* 2014;16:962–975.
14. Wagner C, Polke M, Gerlach RG, et al. Functional dissection of SiiE, a giant non-fimbrial adhesin of Salmonella enterica. *Cell Microbiol* 2011;13:1286–1301.
15. Morgan E, Bowen AJ, Carnell SC, et al. SiiE is secreted by the Salmonella enterica serovar Typhimurium pathogenicity island 4-encoded secretion system and contributes to intestinal colonization in cattle. *Infect Immun* 2007;75:1524–1533.
16. Lorkowski M, Felipe-Lopez A, Danzer CA, et al. Salmonella enterica invasion of polarized epithelial cells is a highly cooperative effort. *Infect Immun* 2014;82:2657–2667.
17. Gerlach RG, Claudio N, Rohde M, et al. Cooperation of Salmonella pathogenicity islands 1 and 4 is required to breach epithelial barriers. *Cell Microbiol* 2008;10:2364–2376.

18. Fink SL, Cookson BT. Pyroptosis and host cell death responses during *Salmonella* infection. *Cell Microbiol* 2007;9:2562–2570.
19. Kim JM, Eckmann L, Savidge TC, et al. Apoptosis of human intestinal epithelial cells after bacterial invasion. *J Clin Invest* 1998;102:1815–1823.
20. Hefele M, Stolzer I, Ruder B, et al. Intestinal epithelial Caspase-8 signaling is essential to prevent necroptosis during *Salmonella Typhimurium* induced enteritis. *Mucosal Immunol* 2018;11:1191–1202.
21. Wemyss MA, Pearson JS. Host cell death responses to non-typhoidal *Salmonella* infection. *Front Immunol* 2019;10:1758.
22. McGuckin MA, Linden SK, Sutton P, et al. Mucin dynamics and enteric pathogens. *Nat Rev Microbiol* 2011;9:265–278.
23. Sheng YH, Hasnain SZ. Mucus and mucins: the underappreciated host defence system. *Front Cell Infect Microbiol* 2022;12:856962.
24. Sheng YH, Hasnain SZ, Florin TH, et al. Mucins in inflammatory bowel diseases and colorectal cancer. *J Gastroenterol Hepatol* 2012;27:28–38.
25. Sheng YH, Lourie R, Lindén SK, et al. The MUC13 cell-surface mucin protects against intestinal inflammation by inhibiting epithelial cell apoptosis. *Gut* 2011;60:1661–1670.
26. McAuley JL, Linden SK, Png CW, et al. MUC1 cell surface mucin is a critical element of the mucosal barrier to infection. *J Clin Invest* 2007;117:2313–2324.
27. McGuckin MA, Every AL, Skene CD, et al. Muc1 mucin limits both *Helicobacter pylori* colonization of the murine gastric mucosa and associated gastritis. *Gastroenterology* 2007;133:1210–1218.
28. Lindén SK, Sheng YH, Every AL, et al. MUC1 limits *Helicobacter pylori* infection both by steric hindrance and by acting as a releasable decoy. *PLoS Pathogens* 2009;5:e1000617.
29. Li X, Bleumink-Pluym NMC, Luijckx Y, et al. MUC1 is a receptor for the *Salmonella* SiiE adhesin that enables apical invasion into enterocytes. *PLoS Pathogens* 2019;15:e1007566.
30. Liu C, Smet A, Blaecher C, et al. Gastric de novo Muc13 expression and spasmolytic polypeptide-expressing metaplasia during *Helicobacter heilmannii* infection. *Infect Immun* 2014;82:3227–3239.
31. LaMonte GM, Orjuela-Sanchez P, Calla J, et al. Dual RNA-seq identifies human mucosal immunity protein Mucin-13 as a hallmark of *Plasmodium exoerythrocytic* infection. *Nat Commun* 2019;10:488.
32. Williams SJ, Wreschner DH, Tran M, et al. Muc13, a novel human cell surface mucin expressed by epithelial and hemopoietic cells. *J Biol Chem* 2001;276:18327–18336.
33. Sheng YH, He Y, Hasnain SZ, et al. MUC13 protects colorectal cancer cells from death by activating the NF-kappaB pathway and is a potential therapeutic target. *Oncogene* 2017;36:700–713.
34. Sheng YH, Triyana S, Wang R, et al. MUC1 and MUC13 differentially regulate epithelial inflammation in response to inflammatory and infectious stimuli. *Mucosal Immunol* 2013;6:557–568.
35. Macao B, Johansson DG, Hansson GC, et al. Autoproteolysis coupled to protein folding in the SEA domain of the membrane-bound MUC1 mucin. *Nat Struct Mol Biol* 2006;13:71–76.
36. Shimamura T, Ito H, Shibahara J, et al. Overexpression of MUC13 is associated with intestinal-type gastric cancer. *Cancer Sci* 2005;96:265–273.
37. Johansson ME, Phillipson M, Petersson J, et al. The inner of the two Muc2 mucin-dependent mucus layers in colon is devoid of bacteria. *Proc Natl Acad Sci U S A* 2008;105:15064–15069.
38. Rodriguez-Pineiro AM, Bergstrom JH, Ermund A, et al. Studies of mucus in mouse stomach, small intestine, and colon: II—gastrointestinal mucus proteome reveals Muc2 and Muc5ac accompanied by a set of core proteins. *Am J Physiol Gastrointest Liver Physiol* 2013;305:G348–G356.
39. Gupta BK, Maher DM, Ebeling MC, et al. Increased expression and aberrant localization of mucin 13 in metastatic colon cancer. *J Histochem Cytochem* 2012;60:822–831.
40. Linden SK, Sutton P, Karlsson NG, et al. Mucins in the mucosal barrier to infection. *Mucosal Immunol* 2008;1:183–197.
41. Ren J, Yan X, Ai H, et al. Susceptibility towards enterotoxigenic *Escherichia coli* F4ac diarrhea is governed by the MUC13 gene in pigs. *PLoS One* 2012;7:e44573.
42. Goetstouwers T, Van Poucke M, Coppieters W, et al. Refined candidate region for F4ab/ac enterotoxigenic *Escherichia coli* susceptibility situated proximal to MUC13 in pigs. *PLoS One* 2014;9:e105013.
43. Schroyen M, Stinckens A, Verhelst R, et al. Susceptibility of piglets to enterotoxigenic *Escherichia coli* is not related to the expression of MUC13 and MUC20. *Anim Genet* 2012;43:324–327.
44. Sinha R, Sahoo NR, Shrivastava K, et al. Resistance to ETEC F4/F18-mediated piglet diarrhoea: opening the gene black box. *Trop Anim Health Prod* 2019;51:1307–1320.
45. Bergstrom KS, Kissoon-Singh V, Gibson DL, et al. Muc2 protects against lethal infectious colitis by disassociating pathogenic and commensal bacteria from the colonic mucosa. *PLoS Pathogens* 2010;6:e1000902.
46. Zarepour M, Bhullar K, Montero M, et al. The mucin Muc2 limits pathogen burdens and epithelial barrier dysfunction during *Salmonella enterica* serovar Typhimurium colitis. *Infect Immun* 2013;81:3672–3683.
47. Barthel M, Hapfelmeier S, Quintanilla-Martinez L, et al. Pretreatment of mice with streptomycin provides a *Salmonella enterica* serovar Typhimurium colitis model that allows analysis of both pathogen and host. *Infect Immun* 2003;71:2839–2858.
48. Hohmann AW, Schmidt G, Rowley D. Intestinal colonization and virulence of *Salmonella* in mice. *Infect Immun* 1978;22:763–770.
49. Furter M, Sellin ME, Hansson GC, et al. Mucus architecture and near-surface swimming affect distinct *Salmonella Typhimurium* infection patterns along the murine intestinal tract. *Cell Rep* 2019;27:2665–2678 e3.
50. Co JY, Margalef-Catala M, Li X, et al. Controlling epithelial polarity: a human enteroid model for host-pathogen interactions. *Cell Rep* 2019;26:2509–2520 e4.

51. Barlag B, Hensel M. The giant adhesin SiiE of *Salmonella enterica*. *Molecules* 2015;20:1134–1150.
52. Bergstrom KS, Xia L. Mucin-type O-glycans and their roles in intestinal homeostasis. *Glycobiology* 2013; 23:1026–1037.
53. Sheng YH, Ng GZ, Summers KM, et al. Influence of the MUC1 cell surface mucin on gastric mucosal gene expression profiles in response to *Helicobacter pylori* infection in mice. *Front Cell Infect Microbiol* 2020; 10:343.
54. Thathiah A, Carson DD. MT1-MMP mediates MUC1 shedding independent of TACE/ADAM17. *Biochem J* 2004;382(pt 1):363–373.
55. Thathiah A, Blobel CP, Carson DD. Tumor necrosis factor-alpha converting enzyme/ADAM 17 mediates MUC1 shedding. *J Biol Chem* 2003;278:3386–3394.
56. Collier-Hyams LS, Zeng H, Sun J, et al. Cutting edge: *Salmonella* AvrA effector inhibits the key proinflammatory, anti-apoptotic NF-kappa B pathway. *J Immunol* 2002;169:2846–2850.
57. Ye Z, Petrof EO, Boone D, et al. *Salmonella* effector AvrA regulation of colonic epithelial cell inflammation by deubiquitination. *Am J Pathol* 2007;171:882–892.
58. Yin C, Liu Z, Xian H, et al. AvrA exerts inhibition of NF-kappaB pathway in its naive *Salmonella* serotype through suppression of p-JNK and Beclin-1 molecules. *Int J Mol Sci* 2020:21.
59. Sheng YH, Wong KY, Seim I, et al. MUC13 promotes the development of colitis-associated colorectal tumors via beta-catenin activity. *Oncogene* 2019; 38:7294–7310.
60. Sellin ME, Muller AA, Felmy B, et al. Epithelium-intrinsic NAIP/NLRC4 inflammasome drives infected enterocyte expulsion to restrict *Salmonella* replication in the intestinal mucosa. *Cell Host Microbe* 2014;16:237–248.
61. Tamaki H, Nakamura H, Nishio A, et al. Human thioredoxin-1 ameliorates experimental murine colitis in association with suppressed macrophage inhibitory factor production. *Gastroenterology* 2006;131:1110–1121.
62. Walsh MD, Young JP, Leggett BA, et al. The MUC13 cell surface mucin is highly expressed by human colorectal carcinomas. *Hum Pathol* 2007;38:883–892.
63. Miyoshi H, Stappenbeck TS. In vitro expansion and genetic modification of gastrointestinal stem cells in spheroid culture. *Nat Protoc* 2013;8:2471–2482.
64. Moon C, VanDussen KL, Miyoshi H, et al. Development of a primary mouse intestinal epithelial cell monolayer culture system to evaluate factors that modulate IgA transcytosis. *Mucosal Immunol* 2014;7:818–828.
65. In JG, Foulke-Abel J, Clarke E, et al. Human colonoid monolayers to study interactions between pathogens, commensals, and host intestinal epithelium. *J Vis Exp* 2019.

Received November 22, 2022. Revised August 25, 2023. Accepted August 28, 2023.

Correspondence

Address correspondence to: Michael McGuckin, PhD, Faculty of Medicine Dentistry and Health Sciences, Alan Gilbert Building, University of Melbourne, Parkville, VIC 3010, Australia. e-mail: Michael.mcguckin@unimelb.edu.au; or Yong Hua Sheng, PhD, Laboratory of B-Lymphocytes in Autoimmunity and Malignancies, QIMR Berghofer Medical Research Institute, Herston, QLD 4006, Australia. e-mail: Yong.Sheng@QIMRBerghofer.edu.au.

Acknowledgments

The authors recognize the technical assistance of the TRI core facilities for histology, flow cytometry, and microscopy. They also thank Ms Madeleine Kersting Flynn from the QIMR Berghofer Medical Research Institute for reformatting the graph abstract.

CRedit Authorship Contributions

Michael A. McGuckin, PhD (Conceptualization: Lead; Data curation: Equal; Formal analysis: Equal; Funding acquisition: Lead; Investigation: Equal; Methodology: Equal; Project administration: Equal; Resources: Lead; Supervision: Equal; Validation: Lead; Visualization: Lead; Writing – review & editing: Lead)

Julie M. Davies, PhD (Data curation: Equal; Validation: Lead; Visualization: Lead; Writing – review & editing: Lead)

Pascal Felgner, PhD (Data curation: Supporting; Formal analysis: Supporting; Methodology: Supporting; Validation: Supporting; Writing – review & editing: Supporting)

Kuan Yau Wong, PhD (Data curation: Equal)

Rabina Giri, PhD (Data curation: Equal)

Yaowu He, PhD (Data curation: Supporting)

Md Moniruzzaman, PhD (Data curation: Supporting)

Thomas Kryza, PhD (Formal analysis: Supporting)

Hareshh Sajir, PhD (Formal analysis: Supporting)

John D. Hooper, PhD (Supervision: Supporting; Validation: Supporting)

Timothy H. Florin, PhD, MD (Supervision: Supporting; Writing – review & editing: Supporting)

Jakob Begun, PhD, MD (Investigation: Supporting; Supervision: Supporting)

Abderrahim Oussalah, PhD, MD (Formal analysis: Supporting; Investigation: Supporting; Supervision: Supporting)

Sumaira Z. Hasnain, PhD (Investigation: Supporting; Supervision: Supporting; Validation: Supporting)

Michael Hensel, PhD (Conceptualization: Supporting; Data curation: Supporting; Investigation: Supporting; Project administration: Supporting; Resources: Supporting; Supervision: Equal; Validation: Equal; Writing – review & editing: Equal)

Yong Hua Sheng, PhD (Conceptualization: Lead; Data curation: Lead; Funding acquisition: Equal; Investigation: Lead; Methodology: Lead; Project administration: Lead; Resources: Equal; Supervision: Lead; Validation: Lead; Visualization: Lead; Writing – original draft: Lead)

Conflicts of interest

The authors disclose no conflicts.

Fundings

Supported by NHMRC project grants 1164141 and 1060698, the Mater Foundation, GESA Project Grant. The Translational Research Institute is supported by a grant from the Federal Government of Australia. MH was supported by the Deutsche Forschungsgemeinschaft by grant P4 in SFB944.